Quantum Theory

HANS DE RAEDT

Institute for Theoretical Physics and Materials Science Centre
University of Groningen, Nijenborgh 4
NL-9747 AG Groningen, The Netherlands
E-mail: deraedt@phys.rug.nl

ABSTRACT

The purpose of this set of lectures is to introduce the general concepts that are at the basis of the computer simulation algorithms that are used to study the behavior of condensed matter quantum systems. The emphasis is on the underlying concepts rather than on specific applications. Topics treated include exact diagonalization techniques, variational methods, Trotter-Suzuki formulae, and Feynman path integrals. Some of the concepts covered are illustrated in an application to electron-phonon models.

1. Introduction

There is a broad consensus that the Schrödinger equation for the time-dependent wave function $|\Phi(t)\rangle$

$$i\hbar\frac{\partial}{\partial t}|\Phi(t)\rangle = H|\Phi(t)\rangle \quad , \tag{1}$$

and the expression for the thermal expectation value of an observable X

$$\langle X\rangle = \frac{Tr\ e^{-\beta H}X}{Tr\ e^{-\beta H}} \quad , \tag{2}$$

describe the dynamic and thermodynamic properties of a system, modelled by a Hamiltonian H, that is in thermal equilibrium at an inverse temperature $\beta = 1/k_BT$. Therefore the rules for formulating the problem are fixed. What remains is to find ways of solving (1) and computing (2).

For classical many-body systems, we can use Molecular Dynamics or Monte Carlo methods to study the model behavior. There are almost no restrictions on the kind of classical models that can be treated in this manner. Unfortunately, for quantum systems the situation is not as good as in the classical case. From numerical point of view, the only "complication" is that, one way or another, quan-

tum mechanics is a theory that is formulated in terms of objects (operators, or, for our purposes, matrices) that do not necessarily commute. This complication has tremendous consequences for it makes the construction and justification of algorithms for simulating quantum systems a difficult task. It is fair to say that at present, there is no quantum simulation method that has the power and general applicability of the techniques developed for classical systems. Consequently it still is a considerable challenge to try to improve existing quantum simulation methods and to invent new ones.

A feeling for the difficulties that arise may be obtained by considering the following example. A model quantum system that has received a lot of attention recently is the so-called Hubbard model. It describes electrons that hop on a lattice. The electrons interact if and only if they are on the same site. Then, by the Pauli principle, they must have opposite spin. For the present discussion, the precise form of the Hamiltonian is irrelevant. Let us try to reduce the quantum problem to a "classical mechanics problem". According to the rules of the game, the only thing we have to do is to solve (1) or, in this case, the time-independent version

$$H|\Phi_n\rangle = E_n|\Phi_n\rangle \quad , \tag{3}$$

where (here and in the following) E_n denotes the n-th eigenvalue of the "matrix" H and $|\Phi_n\rangle$ is the corresponding eigenvector. We will label the eigenvalues such that $E_0 \leq E_1 \leq \ldots \leq E_{M-1}$ where M is the dimension of the matrix H. Now we are in the position to use (2) and compute

$$\langle X\rangle = \sum_{i=0}^{M-1} e^{-\beta E_i}\langle\Phi_i|X|\Phi_i\rangle \Big/ \sum_{i=0}^{M-1} e^{-\beta E_i} \quad , \tag{4}$$

so that in principle, we can solve all model problems.

To see what is really involved to carry out these few steps, we need an order of magnitude for M. For concreteness we will assume that we have a lattice of L sites, filled with $L/2$ electrons with spin up and $L/2$ electrons with spin down. Simple counting shows that

$$M = \binom{L}{L/2}^2 \quad , \tag{5a}$$

which for large L ($L \geq 16$ will do) can be approximated using Stirling's formula to give

$$M \approx \frac{2^{2L+2}}{2\pi L} \quad , \tag{5b}$$

demonstrating that M increases exponentially with $2L$. For instance, if $L = 16$,

$M \approx 10^8$ and for $L = 64$, $M \approx 10^{35}$. To estimate the amount of memory we need to store a single eigenvector we divide (5b) by 2^{27} and obtain

$$MEMORY \approx \frac{2^{2L-25}}{2\pi L} \text{ Gb} \quad , \tag{6}$$

where we have assumed that we need 8 bytes/floating point number. From (6) we see that we need $MEMORY \approx 1$Gb if $L = 16$ whereas for $L = 64$, $MEMORY \approx 10^{28}$Gb ! Although our method of estimating the required amount of memory is somewhat crude, it goes right at the heart of the problem of simulating quantum systems: Where on earth do we find 10^{28}Gb of memory to study a quantum system of only 64 particles on 64 sites ? The basic strategy of any successful quantum simulation technique is to reduce the amount of memory needed at the expense of using (much) more CPU time.

In these lectures we will discuss the general ideas behind quantum simulation methods. The emphasis is on the underlying concepts rather than on specific applications. In section 2, we review methods to compute the ground state properties by exact numerical algorithms, by which we mean that the results are not subject to statistical errors. The amount of storage used is proportional to (5a) . Variational techniques are discussed in section 3. Simulation methods that require $\mathcal{O}(L)$ instead of $\mathcal{O}(2^L)$ memory are based on so-called product formulae which are the subject of section 4. In section 5 we discuss the intimate relationship of these methods with the Feynman path integral formulation of quantum statistical mechanics. Numerical methods for solving the time-dependent Schrödinger equation are introduced in section 6. Finally, in section 7 we show how to construct a Quantum Monte Carlo method for a specific class of electron-phonon models and demonstrate that it can be used to compute static and dynamic properties.

2. Exact Diagonalization

2.1 Methods to compute the full spectrum

Often it is possible to describe the quantum mechanical system by a Hamiltonian that can be represented by a "small" matrix Here "small" means that the dimension of the matrix is such that the whole matrix fits in the memory of the computer at hand. For instance, on a workstation with 128 Mb memory, a "relatively small" system would correspond to a matrix of about 8000×8000. Such matrices can and should be diagonalized using standard linear algebra routines contained in packages such as EISPACK, LAPACK, ESSL, IMSL, etc..

In general, the approach taken in these routines consists of two steps.[1,2] First there is a reduction of the matrix to tri-diagonal form, usually by means of House-

holder transformations. The number of operations for this step is $\mathcal{O}(M^2)$.[1] Then the eigenvalues of the tri-diagonal matrix are found by applying the bisection or the QR algorithm. As solving the eigenvalue problem is equivalent to finding the zero's of the characteristic polynomial, the latter step is an iterative procedure.[1] Typically the number of operations required to compute all the eigenvalues and eigenvectors of a real symmetric matrix is $\mathcal{O}(M^3)$. Evidently, the storage that is needed to hold the matrix or all the eigenvectors is $\mathcal{O}(M^2)$. In practice, one usually runs out of memory long before one has consumed the available CPU time. The usefulness of this approach to solve quantum problems is limited by the amount of available storage and therefore to rather small quantum problems. However it is an essential tool for generating exact results. The latter are of great value for testing other simulation techniques.

2.2 Methods to compute the part of spectrum

Often one is not interested in knowing all the eigenvalues and eigenvectors. For instance, a lot of information on the ground state or zero-temperature ($T = 0$) properties of a quantum system can be computed if the eigenvector corresponding to the smallest eigenvalue is known. One can construct algorithms that are substantially more efficient in terms of memory and CPU usage than full-matrix-diagonalization methods if one focuses on a small part of the spectrum only.

2.2.1 Projector methods

Conceptually, the simplest method to determine the smallest (or largest) eigenvalue and the corresponding eigenvector is the so-called power method.[1] Writing $|\phi\rangle = \sum_{m=0}^{M-1} a_m |\Phi_m\rangle$, the identity

$$\begin{aligned}(E_s - H)^p |\phi\rangle &= \sum_{m=0}^{M-1} a_m (E_s - E_m)^p |\Phi_m\rangle \\ &= (E_s - E_0)^p \left\{ a_0 |\Phi_0\rangle + \sum_{m=1}^{M-1} a_m \left(\frac{E_s - E_m}{E_s - E_0} \right)^p |\Phi_m\rangle \right\} \quad , \end{aligned} \tag{7}$$

shows that repeated application of $E_s - H$ will yield the projection of an arbitrary state $|\phi\rangle$ onto the ground state $|\Phi_0\rangle$, provided the shift E_s is chosen such that $|E_s - E_m|/|E_s - E_0| < 1$, for $m > 0$, and that $\langle\phi|\Phi_0\rangle \neq 0$.

The implementation of this algorithm is straightforward. The storage needed is $\mathcal{O}(M)$. The CPU time per iteration depends on the sparseness of the matrix: For very sparse matrices it is $\mathcal{O}(pM)$. The number of iterations required for convergence to the ground state depends sensitively on the separation between the smallest and next-to-smallest eigenvalue: If the corresponding two states are almost degenerate,

the convergence might be very slow. Then other knowledge, such as model symmetries, can be used to improve the efficiency. The power method is at the heart of the Diffusion Monte Carlo technique where one uses a stochastic process to sample powers of the matrix $E_s - H$.[3]

The idea of using some kind of "filter" to project out the ground state from an initial state is of course quite general. Therefore it is of interest to look for other, more efficient, filters. An obvious choice would be not to use the (shifted) power of H but its inverse. This yields the so-called inverse iteration method which is used in almost all standard packages to compute the eigenvector corresponding to a given eigenvalue.[1,2] The basic idea is the following (we confine ourselves to a discussion for the case where one wants to compute the ground state). Consider the linear equation

$$(H - E_t)|\eta\rangle = |\phi\rangle \quad , \tag{8}$$

where $|\eta\rangle = \sum_{m=0}^{M-1} a_m |\phi_m\rangle$ is an approximation to the ground state $|\Phi_0\rangle$. Then, from (8)

$$|\eta\rangle = (H - E_t)^{-1}|\phi\rangle = \frac{a_0}{E_0 - E_t}|\Phi_0\rangle + \sum_{m=1}^{M-1} \frac{a_m}{E_m - E_t}|\Phi_m\rangle \quad , \tag{9}$$

so that the ground state will give the dominant contribution to η if E_t is close to E_0.

Since the new approximation $|\eta\rangle$ has been obtained by inverting the (almost singular) matrix $H - E_t$ one might wonder about the numerical stability and hence also about the convergence of this scheme. One can prove that inverse iteration does not suffer from the fact that $(H - E_t)^{-1}$ is ill-conditioned: As the length of an eigenvector vector is arbitrary in any case and most of the error is along the direction of the eigenvector that we are looking for, there is no reason for not trusting the result.[2] In practice, there is no need to actually compute the inverse of the matrix $H - E_t$. Instead one solves the linear set of equations (8) directly. The Green Function Monte Carlo technique performs the inverse iteration steps by solving this linear equation by a stochastic method.[3]

Another filter which is frequently used is based on the exponential of the matrix H (for more details about this concept, see below). From the identity

$$\begin{aligned} e^{-\beta H}|\phi\rangle &= \sum_{m=0}^{M-1} a_m e^{-\beta E_m}|\Phi_m\rangle \\ &= e^{-\beta E_0}\left\{ a_0|\Phi_0\rangle + \sum_{m=1}^{M-1} a_m e^{-\beta(E_m - E_0)}|\Phi_m\rangle \right\} \quad , \end{aligned} \tag{10}$$

and our convention that E_0 is the smallest eigenvalue, it is clear that the ground state can be separated from the rest of the spectrum by letting β tend to infinity. More specifically

$$\lim_{\beta\to\infty} \frac{e^{-\beta H}|\phi\rangle}{\sqrt{\langle e^{-\beta H}\phi|e^{-\beta H}\phi\rangle}} = \frac{a_0}{|a_0|}|\Phi_0\rangle \quad . \tag{11}$$

The exponential projector is at the basis of what is called the Projector Quantum Monte Carlo Method. Note that none of the three projector methods will perform well if the ground state is (nearly) degenerate.

2.2.2 Subspace iteration

Both the power and inverse iteration method use information obtained by repeatedly operating with H. It is quite natural to raise the question if there is a way to use this information in a more effective manner, and indeed there is.

Instead of using Householder transformations , one can also use the Lanczos procedure to render the matrix tri-diagonal.[1,2] In general, these two procedures yield two tri-diagonal matrices that will be different although it is evident they do have the same set of eigenvalues and eigenvectors. The numerical stability and efficiency of the Householder method make it the preferred algorithm if a reduction to tri-diagonal form of the full matrix is desired. However, if the matrix is too large to be kept in memory and one is interested in the ground state and perhaps a few excited states only, the Lanczos scheme is the one to use.

The idea behind the Lanczos method is to build a set of orthonormal basis states in such a way that the convergence of the smallest (and also largest) eigenvalues of the 1×1, 2×2, ... sub-matrices is "optimal" in the sense explained below. The first step of the Lanczos algorithm consists in choosing an initial vector (or state) ψ_0 which is assumed to have a nonzero projection onto the (unknown) ground state $|\Phi_0\rangle$. In general, the choice of the starting vector $|\psi_0\rangle$ may affect the rate of convergence of the Lanczos process. For simplicity we assume that $|\psi_0\rangle$ is normalized, i.e. $\langle\psi_0|\psi_0\rangle = 1$. In the second step we compute

$$|\widetilde{\psi}_1\rangle = H|\psi_0\rangle - |\psi_0\rangle\langle\psi_0|H|\psi_0\rangle \quad , \tag{12}$$

so that $\widetilde{\psi}_1$ is orthogonal to ψ_0, i.e. $\langle\psi_0|\psi_1\rangle = 0$. The third step consists of normalizing $\widetilde{\psi}_1$:

$$|\psi_1\rangle = \frac{|\widetilde{\psi}_1\rangle}{\sqrt{\langle\widetilde{\psi}_1|\widetilde{\psi}_1\rangle}} \quad . \tag{13}$$

In the fourth step we construct a vector that is orthogonal to both $|\psi_0\rangle$ and $|\psi_1\rangle$:

$$|\widetilde{\psi}_2\rangle = H|\psi_1\rangle - |\psi_1\rangle\langle\psi_1|H|\psi_1\rangle - |\psi_0\rangle\langle\psi_0|H|\psi_1\rangle \quad , \tag{14}$$

and in the fifth step we normalize $\widetilde{\psi}_2$:

$$|\psi_2\rangle = \frac{|\widetilde{\psi}_2\rangle}{\sqrt{\langle\widetilde{\psi}_2|\widetilde{\psi}_2\rangle}} \quad . \tag{15}$$

Subsequent vectors $|\psi_j\rangle$, for $j = 3, \ldots, M-1$ are generated by repeating the fourth and fifth step, with $|\psi_0\rangle$ replaced by $|\psi_{j-2}\rangle$, $|\psi_1\rangle$ replaced by $|\psi_{j-1}\rangle$, and $|\psi_2\rangle$ replaced by $|\psi_j\rangle$. By construction, $\langle\psi_i|H|\psi_j\rangle = 0$ for all $|i-j| > 1$, i.e. the matrix $T_{i,j} = \langle\psi_i|H|\psi_j\rangle = 0$ is tri-diagonal. The storage required for the vectors and the tri-diagonal matrix is proportional to the dimension M of the Hilbert space.

In contrast to the Householder algorithm, the Lanczos method often suffers from numerical instabilities, resulting from the loss of orthogonality.[1,2] This feature reduces the usefulness of the Lanczos method as a technique to bring the *full* matrix into tri-diagonal form but it has little effect on the accuracy with which the smallest and largest eigenvalues can be found. The reason for this behavior is readily understood by reinterpreting the Lanczos process as a variational technique, as explained in the next section.

In theoretical quantum chemistry, the most popular algorithms to compute a few of the smallest eigenvalues of a large matrix are based on the method proposed by Davidson.[4] The variant I discuss here is taken from the work by J. Olsen *et al.*.[5] Assume that H can be written as $H = A + B$ where B is considered to be a perturbation with respect to A and let $|\psi\rangle$ denote a first (normalized) approximation to the ground state $|\Phi_0\rangle$, so that $E_0 \leq E(\psi) = \langle\psi|H|\psi\rangle$. Write $|\psi'\rangle = |\psi\rangle + |\eta\rangle$ and solve

$$(A+B)(|\psi\rangle + |\eta\rangle) = (E(\psi) + \Delta)(|\psi\rangle + |\eta\rangle) \quad , \tag{16}$$

by keeping terms up to first order in B, Δ, or $|\eta\rangle$ to find

$$|\eta\rangle = -(A - E(\psi))^{-1}\left[(H - E(\psi))|\psi\rangle - \Delta|\psi\rangle\right] \quad . \tag{17}$$

Without loss of generality we can assume that $\langle\psi|\eta\rangle = 0$. Then, from (17) it follows that

$$\Delta = \frac{\langle\psi|(A - E(\psi))^{-1}(H - E(\psi))|\psi\rangle}{\langle\psi|(A - E(\psi))^{-1}|\psi\rangle} \quad . \tag{18}$$

In practice we feed the value for Δ, as calculated from (18), back into (17), replace $|\psi\rangle$ by $|\psi'\rangle$, normalize $|\psi\rangle$, and repeat the procedure. For this method to be useful in practice, there must exist a shortcut to invert the full, large matrix $A - E(\psi)$.

Usually one takes as A the principal $K \times K$ submatrix of H padded with a diagonal matrix consisting of the remaining $M - K$ diagonal elements of H. The dimension K is chosen such that inversion of the $K \times K$ submatrix can be done with standard methods. An advantage of Davidson-based methods over the Lanczos method is that with minor modifications of the scheme outlined above, it is possible to compute the K smallest eigenvalues and corresponding eigenstates without significant loss of accuracy.

3. Variational Methods

3.1 Fundamental Theorems

All variational methods for solving quantum problems are based on a fundamental result of Poincaré called the minimax characterization of the eigenvalues.[1,2] One way of stating this result is to say that the j-th eigenvalue E_j for $j = 0, \ldots, M-1$ can be calculated as

$$E_j = min \underset{\psi \in S_{j-1}}{max} R(H, \psi) \quad , \tag{19}$$

where

$$R(H, \psi) = \frac{\langle \psi | H | \psi \rangle}{\langle \psi | \psi \rangle} \quad , \tag{20}$$

denotes the Rayleigh quotient, and S_{j-1} is the set $|\psi\rangle$'s, subject to all possible $j-1$ linear constraints. Application of this theorem to the case of the ground state of the quantum system yields the well-known variational principle:

$$E_0 \leq \frac{\langle \psi | H | \psi \rangle}{\langle \psi | \psi \rangle} \quad , \tag{21}$$

for any choice of $|\psi\rangle \neq 0$.

For later use we mention here another equally important result due to Cauchy.[2] It relates the eigenvalues of a principal submatrix to those of the full matrix. To be precise let

$$H = \begin{pmatrix} H^{(k)} & X^T \\ X & Y \end{pmatrix} \quad , \tag{22}$$

where $k \leq M - 1$. Then, for $j = 0, \ldots, k$

$$E_j \leq E_j^{(k)} \leq E_{M-k+j} \quad , \tag{23}$$

where $E_j^{(k)}$ denotes the j-th eigenvalue of the matrix $H^{(k)}$. Note that (23) also makes statements about the excited states. If $k = M - 1$, Cauchy's results is also known as the separation theorem.[1,2]

3.2 Trial State Approach

The most straightforward application of result (21) consists of making an ansatz for the trial function $|\psi\rangle = |\psi(\{\alpha_j\})\rangle$ where $\{\alpha_j\}$ denotes a set of parameters that are used to minimize the r.h.s. of (21). In practice, the usefulness of this approach crucially depends on two factors. First of all, for any choice of $\{\alpha_j\}$, it should be possible to compute the matrix elements

$$R(H, \{\alpha_j\}) = \frac{\langle\psi(\{\alpha_j\})|H|\psi(\{\alpha_j\})\rangle}{\langle\psi(\{\alpha_j\})|\psi(\{\alpha_j\})\rangle} \quad . \tag{24}$$

For a non-trivial many-body system it is not a simple matter to evaluate these matrix elements analytically and one usually has to resort to Monte Carlo techniques to evaluate (the ratio of) these matrix elements. Secondly, the form of $|\psi(\{\alpha_j\})\rangle$ should be flexible enough to cover the essential physics of the system. It is clear that making an appropriate choice for the form of $|\psi(\{\alpha_j\})\rangle$ requires detailed knowledge about the behavior of the system, possibly biasing the results of the calculation. Appealing features of this approach are its simplicity and its general applicability to continuum and lattice models.

3.3 Recursive Variational Techniques

A simple choice for the form of ψ, allowing for systematic improvements, is given by

$$|\psi\rangle = \sum_{j=0}^{k-1} \alpha_j |\phi_j\rangle \quad , \tag{25}$$

where $\{|\phi_j\rangle\}$ is a complete set of basis vectors and the α_j's are the minimization parameters. Minimization of the Rayleigh quotient is equivalent to the calculation of the smallest eigenvalue of the principal $k \times k$ matrix $H^{(k)}$. The separation theorem tells us that by including another basis state $|\phi_k\rangle$ and corresponding coefficient α_k, we can improve the approximation since

$$E_0 \leq E_0^{(k+1)} \leq E_0^{(k)} \quad . \tag{26}$$

This result is the basis of the Lanczos-based techniques for computing the ground state of a quantum system. Consider the Lanczos process after k states have been generated. The set of states $\{\psi_0, \ldots, \psi_{k-1}\}$ fully qualifies as a set of basis states.

Diagonalizing the $k \times k$ tri-diagonal matrix yields $E_0^{(k)}$. According to (26), performing one more Lanczos step, followed by another diagonalization of the new tri-diagonal matrix will yield a better approximation to the ground state energy. The power of the Lanczos scheme stems from the fact that, on the basis of all the information on the eigenvalues already contained in the k-dimensional subspace spanned by $\{|\psi_0\rangle, \ldots, |\psi_{k-1}\}\rangle$, the next Lanczos step is the best thing one can do to improve the approximation. To see this, compute the gradient of the Rayleigh quotient to find

$$\frac{\partial R(H,\psi)}{\partial \alpha_j} \propto \langle \phi_j | \big[H|\psi\rangle - |\psi\rangle\langle\psi|H|\psi\rangle \big] \rangle \quad , \tag{27}$$

showing that the vector required in the $(k+1)$-th step of the Lanczos process, is parallel to the vector that specifies the direction for minimizing the Rayleigh quotient.[6]

The fact that each step of the Lanczos process can be viewed as an attempt to minimize the Rayleigh quotient suggest that in practice, the calculation of the ground state can be rearranged such that there is no need to explicitly diagonalize the tri-diagonal matrix. We will illustrate this idea by combining the steepest descent and Lanczos technique.[7] Assume we have already carried out k iterations, i.e. we know the trial state $|\psi\rangle$. According to the Lanczos procedure, the next step is to compute the new vector

$$|\psi'\rangle = \frac{H|\psi\rangle - |\psi\rangle\langle\psi|H|\psi\rangle}{\sqrt{\langle\psi|H^2|\psi\rangle - \langle\psi|H|\psi\rangle^2}} \quad . \tag{28}$$

Minimizing the Rayleigh quotient with respect to the trial state $x|\psi\rangle + y|\psi'\rangle$ amounts to solving eigenvalue problem for the two-by-two matrix

$$A = \begin{pmatrix} \langle\psi|H|\psi\rangle & \langle\psi|H|\psi'\rangle \\ \langle\psi'|H|\psi\rangle & \langle\psi'|H|\psi'\rangle \end{pmatrix} \quad . \tag{29}$$

The eigenvector (x_0, y_0) corresponding to the smallest eigenvalue of A is then used to construct the new trial state $|\psi\rangle \leftarrow x_0|\psi\rangle + y_0|\psi'\rangle$ that serves as input for the next iteration.

Steepest descent is only one of the many techniques that can be used to minimize the Rayleigh quotient. In general it is not very efficient but it is simple to program. A slightly more complicated approach that is similar in spirit and more efficient in terms of the number of iterations uses a combination of Lanczos steps and conjugate gradient minimization.[8]

The salient features of all these recursive variational algorithms are that 1) in principle, they will yield the exact ground state for a sufficiently large number of iterations, 2) the storage during the iterations is proportional to the dimension M of

the full Hilbert space, and 3) there is no general recipe for determining the number of iterations that will be required.

3.4 Stochastic Diagonalization

For many problems of interest the dimension of the Hilbert space becomes so large that it is no longer feasible to store even a single vector. Then, the only way to make progress towards solving the problem is to make the basic assumption that of the whole, large set of basis vectors, only a relatively small portion is important when it comes to computing physical properties. Instead of using the sparseness of the matrix, we will now assume that the solution itself is "sparse" in the sense that only a small fraction of the elements of the eigenvector, corresponding to the smallest eigenvalue, is non-zero.

The stochastic diagonalization algorithm (SD) implements this idea in the following way.[9,10] We know that the ground state can be written as a linear combination of all the basis states (to keep the discussion as simple as possible no use will be made of the model symmetry to reduce the size of the Hilbert space):

$$|\Phi_0\rangle = \sum_{j=0}^{M-1} c_j |\phi_j\rangle \quad . \tag{30}$$

In principle we can rearrange the terms in this sum so that the ones with the largest amplitude are in front:

$$|\Phi_0\rangle = \sum_{j=0}^{M-1} c_{Pj} |\phi_{Pj}\rangle \quad . \tag{31}$$

Here P denotes the permutation of the set $\{0, \ldots, M-1\}$ such that $|c_{Pj}| \geq |c_{P(j+1)}|$. Assuming that we obtain a good approximation if we restrict the sum to the first M_I terms we have

$$|\Phi_0\rangle \approx |\widetilde{\Phi}_0\rangle = \sum_{j=0}^{M_I} c_{Pj} |\phi_{Pj}\rangle \quad . \tag{32}$$

By virtue of the Poincaré theorem we have

$$E_0 \leq \widetilde{E}_0 = \frac{\langle \widetilde{\Phi}_0 | H | \widetilde{\Phi}_0 \rangle}{\langle \widetilde{\Phi}_0 | \widetilde{\Phi}_0 \rangle} \quad , \tag{33}$$

demonstrating that stochastic diagonalization belongs to the class of variational techniques. In general we can only hope that $M_I \ll M$ and in practice M_I will depend on the actual choice of the basis vectors and on the matrix H. Note that the

SD method will yield the exact result whenever other methods (such as Lanczos) will, because then we can store the whole vector and put $M_I = M$ from the start.

Up to know, we have assumed that we know the permutation P that does the job described above, but in fact we don't know P nor do we know the coefficients c_{Pj}. The crux of the SD method is that it uses a stochastic process to construct P and the coefficients c_{Pj} simultaneously. Thereby it does not suffer from the so-called minus-sign problem (to be discussed below) that is usually encountered in Quantum Monte Carlo work. A detailed description of the SD method is beyond the scope of these lectures. A rigorous proof of the correctness of the SD algorithm, an extensive discussion on the origin of the minus-sign problem, details on the implementation of the SD algorithm, and applications to the Hubbard model can be found elsewhere.[10] Some application to quantum chemistry problems is given in ref. 11 .

3.5 Computation of physical properties

In quantum mechanics, physical quantities are related to matrix elements of physical observables (Hermitian matrices for our purposes). Assuming the ground state wave function has been obtained, for instance by one of the methods described above, the calculation of these matrix elements itself becomes a non-trivial problem if the matrix representing the observable is not diagonal in the basis that was used to diagonalize the Hamiltonian. Indeed, if A denotes the physical observable,

$$\langle A \rangle = \langle \Phi_0 | A | \Phi_0 \rangle = \sum_{i,j=0}^{M-1} c_i c_j \langle \phi_i | A | \phi_j \rangle \quad , \tag{34}$$

showing that in general it will take $\mathcal{O}(M^2)$ operations to carry out this computation. For large M, it may take longer to calculate certain expectation values than it takes to solve for the ground state by one of the variational methods described above. Finally, it is important to keep in mind that a variational calculation that yields a good approximation to the energy can be quite bad for other physical quantities. This is most evident in the case where the ground state is (nearly) degenerate, but care has to be taken in other cases as well.

4. Trotter-Suzuki Formulae

In analogy with ordinary differential equations, the formal solution of the differential equation

$$\frac{\partial}{\partial \lambda} U(\lambda) = H U(\lambda) \quad ; \quad U(0) = I \quad , \tag{35}$$

where H is a $M \times M$ matrix, is given by

$$U(\lambda) = e^{\lambda H} \quad , \tag{36}$$

and is called the exponential of the matrix H. In quantum physics and quantum statistical mechanics, the exponential of the Hamiltonian is a fundamental quantity. All methods for solving these problems compute, one way or another, (matrix elements of) the exponential of the matrix H. For our purposes, $\lambda = -\beta = -1/k_B T$ for quantum statistical problems and $\lambda = -it/\hbar$ for the case of real time quantum dynamics. Formally, the exponential of a matrix H can be defined in terms of the Taylor series

$$e^{\lambda H} = \sum_{n=0}^{\infty} \frac{\lambda^n}{n!} H^n \quad , \tag{37}$$

just like if H would be a number. For most problems of interest, there won't be enough memory to store the matrix H and hence there also will be no memory to store the full matrix $e^{\lambda H}$. So let us concentrate on the other extreme: The calculation of an arbitrary matrix element $\langle \psi | e^{\lambda H} | \psi' \rangle$. Although from mathematical point of view, formal expansion (37) is all that is really needed, when it comes to computation, (37) is quite useless. The reason is not so much that it is a Taylor series but rather that it contains powers of the matrix, indicating that simply summing the terms in (37) may be very inefficient (and indeed it is).

There is one particular case in which it is easy to compute the matrix element $\langle \psi | e^{\lambda H} | \psi' \rangle$ namely if all the eigenvalues and eigenvectors are known. Indeed, from (37) it follows that

$$e^{\lambda H} |\Phi_j\rangle = \sum_{n=0}^{\infty} \frac{\lambda^n}{n!} H^n |\Phi_j\rangle = \sum_{n=0}^{\infty} \frac{\lambda^n}{n!} E_j^n |\Phi_j\rangle = e^{\lambda E_j} |\Phi_j\rangle \quad , \tag{38}$$

so that

$$\langle \psi | e^{\lambda H} | \psi' \rangle = \sum_{j=0}^{M-1} \langle \psi | \Phi_j \rangle \langle \Phi_j | \psi' \rangle e^{\lambda E_j} \quad . \tag{39}$$

Of course, result (39) is almost trivial but it is important to keep in mind that, except for some pathological cases, there seems to be no other practical way to compute the matrix element $\langle \psi | e^{\lambda H} | \psi' \rangle$ without making approximations (assuming H is a large matrix). In general we don't know the solution of the eigenvalue problem of the matrix H, otherwise we would already have solved the most difficult part of the whole problem. Therefore (39) is not of practical use.

In all cases that we know of, the Hamiltonian is a sum of several contributions and each contribution itself is usually simple enough so that we can diagonalize

it ourselves by some (simple) transformation. The Hamiltonian for a particle in a potential provides the most obvious example: We can write the Hamiltonian as a sum of the free-particle Hamiltonian and a potential energy. It is trivial to diagonalize both parts independently but it is usually impossible to diagonalize the sum.

The question we can now put ourselves is the following. Suppose we can diagonalize each of the terms in H by hand. Then, it is very reasonable to assume that we can also compute the exponential of each of the contributions separately (see (39)). Is there then a relation between the exponentials of each of the contributions to H and the exponential of H and if so, can we use it to compute the latter ?

The answer to this question is affirmative and can be found in the mathematical literature of the previous century. The following fundamental result due to Lie,[12] is the basis for the Trotter-Suzuki method for solving quantum problems.[13,14,15] It expresses the exponential of a sum of two matrices as infinite ordered product of the exponentials of the two individual matrices:

$$e^{\lambda(A+B)} = \lim_{m\to\infty} \left(e^{\lambda A/m} e^{\lambda B/m}\right)^m \quad , \tag{40}$$

where, for our purposes, A and B are $M \times M$ matrices. The result (40) is called the Trotter formula. A first hint for understanding why (40) holds comes from comparing the two Taylor series

$$\begin{aligned} e^{\lambda(A+B)/m} &= 1 + \frac{\lambda}{m}(A+B) + \frac{1}{2}\frac{\lambda^2}{m^2}(A+B)^2 + \mathcal{O}(\lambda^3/m^3) \\ &= 1 + \frac{\lambda}{m}(A+B) \\ &\quad + \frac{1}{2}\frac{\lambda^2}{m^2}(A^2 + AB + BA + B^2) + \mathcal{O}(\lambda^3/m^3) \quad , \end{aligned} \tag{41a}$$

and

$$e^{\lambda A/m} e^{\lambda B/m} = 1 + \frac{\lambda}{m}(A+B) + \frac{1}{2}\frac{\lambda^2}{m^2}(A^2 + 2AB + B^2) + \mathcal{O}(\lambda^3/m^3) \quad . \tag{41b}$$

It is clear that for sufficiently large m, both expansions will agree up to terms of $\mathcal{O}(\lambda^2\|[A,B]\|/m^2)$. Thus, for sufficiently large m (how large depends on λ and $\|[A,B]\|$),

$$e^{\lambda(A+B)/m} \approx e^{\lambda A/m} e^{\lambda B/m} \quad . \tag{42}$$

A mathematically rigorous treatment shows that[16]

$$\|e^{\lambda(A+B)} - \left(e^{\lambda A/m} e^{\lambda B/m}\right)^m\| \leq \frac{\lambda^2}{2m}\|[A,B]\| e^{|\lambda|(\|A\|+\|B\|)} \quad , \tag{43}$$

demonstrating that for finite m, the difference between the exponential of a sum of two matrices and the ordered product of the individual exponentials vanishes as λ^2/m. As expected, (43) also reveals that this difference is zero if A and B commute: If $[A,B]=0$ then $e^{\lambda(A+B)}=e^{\lambda A}e^{\lambda B}$.

Except for the fact that we assumed that $H=A+B$, the above discussion has been extremely general. This suggests that one can apply the Trotter-Suzuki approach to a wide variety of problems and indeed one can. We have only discussed the most simple form of the Trotter formula. There now exist a vast number of extensions and generalizations of which we will consider only one in this section, and another one in the section on quantum dynamics.

The Trotter formula is readily generalized to the case of more than two contributions to H. Writing $H=\sum_{i=1}^{p}A_i$ it can be shown that[16]

$$\| \, exp\left[\lambda\sum_{i=1}^{p}A_i\right]-\left(e^{\lambda A_1/m}\ldots e^{\lambda A_p/m}\right)^m \, \| \leq \frac{\lambda^2}{2m}\sum_{1\leq i<j\leq p}\|[A_i,A_j]\| \, exp\left[|\lambda|\sum_{i=1}^{p}\|A_i\|\right] \quad , \tag{44}$$

showing that *any* decomposition of the Hamiltonian qualifies as a candidate for applying the Trotter-Suzuki approach. This is an important conclusion because the flexibility of choosing the decomposition of H can be exploited to construct efficient algorithms. From the above discussion it is also clear that at no point, an assumption was made about the "importance" of a particular contribution to H. Therefore the Trotter-Suzuki approach can be used where perturbation methods break down.

Trotter-Suzuki formulae provide an extremely powerful setting for constructing whole families of algorithms to compute matrix elements of the exponential of H. We will illustrate their use by concentrating on the simplest example where we decompose the Hamiltonian H in two parts $H=A_1+A_2$. Using (40) the partition function can be written as

$$Z = Tr \; e^{-\beta H} = Tr \; e^{-\beta(A_1+A_2)} = \lim_{m\to\infty} Z_m \quad , \tag{45a}$$

where

$$Z_m = Tr \; \left(e^{-\beta A_1/m}e^{-\beta A_2/m}\right)^m \quad , \tag{45b}$$

denotes the m-th approximant to the partition function Z. In numerical work, it is impossible to take the limit $m\to\infty$. Therefore, the general strategy of the Trotter-Suzuki approach is to compute the m-th approximant for various m, to study the convergence as a function of m, and to extrapolate to $m\to\infty$. Recall

that convergence is guaranteed by inequalities such as (43) and (44).

We can compute Z_m as follows. By construction we may assume (see above) that we already know the eigenvalues $E_j^{(p)}$ and eigenvectors $|\Phi_j^{(p)}\rangle$ of the matrices A_p, for $p = 1, 2$. Since each set of eigenvectors form a complete set of states, the identity matrix I can be expressed as

$$\sum_{j=0}^{M-1} |\Phi_j^{(p)}\rangle\langle\Phi_j^{(p)}| = I \quad ; \quad p = 1, 2 \quad . \tag{46}$$

Using representation (46), the approximant (45b) can be written as

$$\begin{aligned} Z_m =& Tr\ \left(e^{-\beta A_1/m}\, I\, e^{-\beta A_2/m}\, I\right)^m \\ =& \sum_{\{j_n\}} \sum_{\{k_n\}} \prod_{n=1}^{m} \langle\Phi_{j_n}^{(2)}|e^{-\beta A_1/m}|\Phi_{k_n}^{(1)}\rangle\langle\Phi_{k_n}^{(1)}|e^{-\beta A_2/m}|\Phi_{j_{n+1}}^{(2)}\rangle \\ =& \sum_{\{j_n\}} \sum_{\{k_n\}} \prod_{n=1}^{m} exp\left[-\beta\left(E_{k_n}^{(1)} + E_{j_n}^{(2)}\right)/m\right] \langle\Phi_{j_n}^{(2)}|\Phi_{k_n}^{(1)}\rangle\langle\Phi_{k_n}^{(1)}|\Phi_{j_{n+1}}^{(2)}\rangle \quad , \end{aligned} \tag{47}$$

subject to the boundary condition $j_{m+1} = j_1$, reflecting the fact that we are calculating the trace of a matrix.

Expressions similar to (47) for the m-th approximant to any expectation value of interest can be obtained by repeating the steps that lead to (47). The general, the m-th approximant to the expectation value of an observable X can be written as

$$\langle X\rangle_m = \frac{\sum_{\{j_n\}} \sum_{\{k_n\}} \rho(\{j_n\},\{k_n\}) X(\{j_n\},\{k_n\})}{\sum_{\{j_n\}} \sum_{\{k_n\}} \rho(\{j_n\},\{k_n\})} \quad , \tag{48a}$$

where

$$\rho(\{j_n\},\{k_n\}) = \prod_{n=1}^{m} e^{-\beta\left(E_{k_n}^{(1)} + E_{j_n}^{(2)}\right)/m} \langle\Phi_{j_n}^{(2)}|\Phi_{k_n}^{(1)}\rangle\langle\Phi_{k_n}^{(1)}|\Phi_{j_{n+1}}^{(2)}\rangle \quad , \tag{48b}$$

For fixed m, the calculation of (48a) is straightforward, at least in principle: All quantities are known so we just have to sum over all M^{2m} possibilities. In practice, the number of possibilities can become so large that it is not feasible to sum all terms. Then an importance sampling method such as the Metropolis Monte Carlo or a Molecular Dynamics technique can be used to estimate the m-th approximant to thermal expectation values. Simulation techniques based on these ideas are called Quantum Monte Carlo methods.[13,14,15]

Although from the derivation given above, it may look as if the additional

M^{2m-1} degrees of freedom are the only extra's one pays for transforming the quantum statistical problem into a "classical" mechanics problem, there is a fundamental problem with this approach.[10,13,15] Indeed, the presence in (48b) of the matrix elements of the eigenstates $|\Phi_j^{(p)}\rangle$ implies that one cannot exclude that in general, there may exist combinations of the labels $\{j_n\}$ and $\{k_n\}$ for which $\rho(\{j_n\},\{k_n\})$ is zero, negative or even complex. This phenomenon is often referred to as the "minus-sign" problem.[10,13,15] The usefulness of a Quantum Monte Carlo method is reduced considerably when minus-sign problems are encountered.

The class of quantum systems that does not suffer from minus-sign problems is rather small. One can show that if all non-diagonal matrix elements of H are negative there will be no minus sign problems (obviously, the sign of the matrix elements depends on the choice of the basis vector $|\phi_j\rangle$).[10] This sufficient condition applies not only to Trotter-Suzuki based methods but also to the Diffusion, Green Function, and Projector Quantum Monte Carlo techniques as well. An in-depth discussion of the minus-sign problem can be found elsewhere.[10] For the present purpose, it is sufficient to know that it is a fundamental problem resulting from the use of a product formula (in practice projection-based methods are product formulae in disguise) and conventional importance sampling techniques.[10] Therefore the minus-sign problems is an intrinsic property of this approach to solving quantum problems and, contrary to the common lore, due to the presence of fermionic degrees of freedom.[15] Sometimes, it is possible to perform the sum (or integration) over some of the degrees of freedom analytically. Usually it pays off to reduce the numerical work by analytical manipulations, in particular if one can eliminate the minus-sign problem (an example is given in the last section). Methods that are free of minus-sign problems are the exact diagonalization techniques, the trial-state approach and the stochastic diagonalization method.

5. Path Integrals

For a particular class of model Hamiltonians, $lim_{m\to\infty} Z_m$ reduces to the Feynman path integral representation of the partition function. Usually, Feynman's path integral is obtained by starting from the expression of the classical action and allowing for particle trajectories other than the classical one. The Trotter-Suzuki formula gives a precise prescription of how such a path integral can be constructed. From mathematical perspective, the Trotter-Suzuki approach for approximating exponentials of matrices is much more general than the Feynman path integral: It can be used for model Hamiltonians (matrices, linear operators) for which it is apparently impossible to write down the classical action.[13]

We will illustrate the construction of the Feynman path integral for the generic Hamiltonian

$$H = \sum_{i=1}^{N} \frac{p_i^2}{2m^*} + \sum_{1 \le i < j \le N} V(r_i, r_j) \quad , \tag{49}$$

where p_i and r_i denote the momentum and position operator of the i-th particle. The particles have mass m^* and interact via a potential $V(r_i, r_j)$. For simplicity we will assume that they are distinguishable. Treating fermion or boson systems requires only minor modifications.[13,17] We decompose the Hamiltonian (49) into kinetic and potential energy. The eigenstates of the kinetic energy are direct products of free-particle eigenstates. Writing $|q_1, \ldots, q_N\rangle$ for $|\Phi_k^{(1)}\rangle$ where $p_i|q_i\rangle = \hbar q_i |q_i\rangle$, and $|x_1, \ldots, x_N\rangle$ for $|\Phi_j^{(2)}\rangle$ where $r_i|x_i\rangle = x_i|x_i\rangle$, the first factor in the product of matrix elements (4.13) reads

$$\begin{aligned}
&\langle x_1, \ldots, x_N| \, exp\left(-\frac{\beta}{2m^* m} \sum_{i=1}^{N} p_i^2\right) |x_1', \ldots, x_N'\rangle \\
&\quad = \int_{-\infty}^{+\infty} dq_1 \ldots dq_N \, \langle x_1, \ldots, x_N| \, exp\left(-\frac{\beta}{2m^* m} \sum_{i=1}^{N} p_i^2\right) |q_1, \ldots, q_N\rangle \\
&\qquad\qquad \times \langle q_1, \ldots, q_N | x_1', \ldots, x_N'\rangle \\
&\quad = \int_{-\infty}^{+\infty} dq_1 \ldots dq_N \, \langle x_1, \ldots, x_N | q_1, \ldots, q_N\rangle \langle q_1, \ldots, q_N | x_1', \ldots, x_N'\rangle \\
&\qquad\qquad \times exp\left(-\frac{\beta}{m} \sum_{i=1}^{N} \frac{\hbar^2 q_i^2}{2m^*}\right) \\
&\quad = \int_{-\infty}^{+\infty} dq_1 \ldots dq_N \, \prod_{j=1}^{N} e^{i(x_j - x_j')\cdot q_j} e^{-\beta \hbar^2 q_j^2 / 2m^* m} \quad ,
\end{aligned} \tag{50}$$

where, in the last step, we used $\langle x_j | q_j \rangle = e^{i x_j \cdot q_j}$. Using the fact that the potential energy is diagonal when we work in the coordinate representation, the second factor in (4.13) takes the form

$$\begin{aligned}
&\langle x_1, \ldots, x_N| \, exp\left(-\frac{\beta}{m} \sum_{1 \le i < j \le N} V(r_i, r_j)\right) |x_1', \ldots, x_N'\rangle \\
&\qquad = exp\left(-\frac{\beta}{m} \sum_{1 \le i < j \le N} V(x_i, x_j)\right) \prod_{i=1}^{m} \delta(x_i - x_i') \quad .
\end{aligned} \tag{51}$$

The identity

$$\int_{-\infty}^{+\infty} e^{-ay^2+by}\,dy = \sqrt{\frac{\pi}{a}} e^{b^2/4a} \quad , \tag{52}$$

allows the integrals over all q_j in (51) to be worked out analytically, giving

$$Z_m = \left(\frac{2\pi m^* m}{\beta\hbar^2}\right)^{d/2} \int_{-\infty}^{+\infty} dx_{1,n}\ldots dx_{N,m}\, exp\left\{-\frac{m^* m}{2\beta\hbar^2}\sum_{n=1}^{m}\sum_{j=1}^{N}(x_{j,n}-x_{j,n+1})^2 \right.$$
$$\left. -\frac{\beta}{m}\sum_{n=1}^{m}\sum_{1\le i<j\le N} V(x_{i,n},x_{j,n})\right\} \quad , \tag{53}$$

where d denotes the dimension of the space in which the particles move. Using

$$\lim_{m\to\infty}\frac{m}{\beta}\sum_{n=1}^{m}(x_{j,n}-x_{j,n+1})^2 = \lim_{m\to\infty}\frac{\beta}{m}\sum_{n=1}^{m}\left(\frac{x_{j,n}-x_{j,n+1}}{\beta/m}\right)^2$$
$$= \int_0^\beta d\tau\,\left(\frac{dx_j(\tau)}{d\tau}\right)^2 \quad , \tag{54a}$$

and

$$\lim_{m\to\infty}\frac{\beta}{m}\sum_{n=1}^{m} V(x_{i,n},x_{j,n}) = \int_0^\beta d\tau\, V(x_i(\tau),x_j(\tau)) \quad , \tag{54b}$$

we recover the Feynman path integral representation of the partition function

$$Z = \int \mathcal{D}x(\tau)\, e^{-S(\{x_j(\tau)\})} \quad , \tag{55}$$

where for model (50)

$$S(\{x_j(\tau)\}) = \frac{m^*}{2}\sum_{j=1}^{N}\int_0^\beta d\tau\,\left(\frac{dx_j(\tau)}{d\tau}\right)^2 + \sum_{1\le i<j\le N}\int_0^\beta d\tau\, V(x_i(\tau),x_j(\tau)) \quad , \tag{56}$$

is the classical action of the N particles, moving along the path $\{x_j(\tau)\}$ parameterized by the imaginary time τ. To obtain the real-time Feynman path integral replace β by $it/\hbar$.

The Feynman path integral (56) and its interpretation in terms of particles moving along world lines carries over to (53). First we make m replicas of the original physical system. Then we connect the coordinates with the same particle label by harmonic springs (the first term in the exponential appearing in (53)), restricting the connections to replica's that are nearest neighbors with respect to the replica label n. Within each replica the particles interact with each other via

potential $V(x,x')$. The forces resulting from the springs get stronger as $m \to \infty$ or $k_B T = 1/\beta \to 0$, while the forces due to $V(x,x')$ get weaker (note that we have to let $m \to \infty$ before we let $\beta \to \infty$ to recover the exact result). The fact that these interactions depend on m, the size of the system in the imaginary-time direction, indicates that the interpretation of (53) as a partition function of some genuine classical system is somewhat misleading.[13]

6. Quantum Dynamics

In this section we will discuss numerical algorithms to solve the TDSE

$$i\hbar \frac{\partial}{\partial t} |\Phi(t)\rangle = \mathcal{H} |\Phi(t)\rangle \quad , \tag{57}$$

where $|\Phi(t)\rangle$ represents the state of the system described by the Hamiltonian $\mathcal{H}$ (in this section we use $\mathcal{H}$ for the differential operator and H for the corresponding matrix). Solving the time-dependent Schrödinger equation for a single particle moving in a non-trivial (electromagnetic) potential is not a simple matter. The main reason is that for most problems of interest, the dimension of the matrix representing $\mathcal{H}$ can be quite large. Typical applications use matrices of dimension $M = 10^6$ or larger. Although the dimension of the matrices involved is certainly not as large as in the case of typical many-body quantum systems, exact diagonalization techniques quite useless. Indeed, a calculation of the time-development of the wave function by exact diagonalization techniques requires the knowledge of *all* eigenvectors and *all* eigenvalues (i.e. $\approx 10^{13}$ Mb or more RAM to store these data). Thus, we need algorithms that do not use more than $\mathcal{O}(M+1)$ storage elements but the diagonalization methods discussed above are of very limited use. Methods based on importance sampling concepts cannot be employed either because there is no criterion to decide which state is important or which is not.

A key concept in the construction of an algorithm for solving the TDSE is the so-called unconditional stability. An algorithm for solving the TDSE is unconditionally stable if the norm of the wavefunction is conserved *exactly*, at *all* times.[18] From physical point of view, unconditional stability obviously is an essential requirement. If an algorithm is unconditionally stable the errors due to rounding, discretization etc. never run out of hand, irrespective of the choice of the grid, the time step, or the number of propagation steps. Recall that the formal solution of the TDSE is given by

$$|\Phi(m\tau)\rangle = e^{-im\tau\mathcal{H}} |\Phi(t=0)\rangle \quad , \tag{58}$$

where $m = 0, 1, \ldots$ counts the number of time-steps τ.

A simple, general recipe for constructing an unconditionally stable algorithm is to use unitary approximations to the (unitary) time-step operator $U(\tau) = e^{-i\tau\mathcal{H}}$.[18]

Trotter-Suzuki formulae provide the necessary mathematical framework for constructing unconditionally stable, accurate and efficient algorithms to solve the TDSE.[18] For many applications it is necessary to employ an algorithm that is correct up to fourth order, both in space and time. Trotter-Suzuki formula-based procedures to devise algorithms that are correct up to fourth-order in the time step are given in ref.18. From practical point of view, a disadvantage of the fourth-order methods introduced in ref.18 is that they involve commutators of various contributions to the Hamiltonian. Recently Suzuki proposed a symmetrized fractal decomposition of the time evolution operator.[19] Using this formula, a fourth-order algorithm is easily built from a second-order algorithm by applying[19]

$$U_4(\tau) = U_2(p\tau)U_2(p\tau)U_2((1-4p)\tau)U_2(p\tau)U_2(p\tau) \quad , \tag{59}$$

where $p = 1/(4 - 4^{1/3})$ and $U_n(\tau)$ is the n–th order approximation to $U(\tau)$, i.e. $U(\tau) = U_n(\tau) + \mathcal{O}(\tau^{n+1})$. Approximants correct up to second order are obtained by symmetrization of first order approximants,[18,19,20] namely

$$U_2\ (\tau) = U_1^T(\tau/2)U_1\ (\tau/2) \quad , \tag{60}$$

where the U_1^T is the transpose of U_1 .

Usually the Hamiltonian can be written as a sum of different contributions which may or may not commute. The first-order approximant $U_1(\tau)$, corresponding to the decomposition

$$\mathcal{H} = \sum_{n=1}^{N} \mathcal{H}_n \quad , \tag{61a}$$

is given by

$$U_1(\tau) = e^{-i\tau\mathcal{H}_1}\, e^{-i\tau\mathcal{H}_2} \ldots e^{-i\tau\mathcal{H}_N} = \prod_{n=1}^{N} e^{-i\tau\mathcal{H}_n} \quad . \tag{61b}$$

In general there will be many possibilities to write down different decompositions of a given Hamiltonian. From theoretical point of view, the choice of the decomposition is arbitrary. In practice however, this flexibility can be exploited to considerable extent to tailor the algorithm to the computer architecture on which the algorithm will execute. Of particular interest are decompositions that vectorize well and have a large intrinsic degree of parallelism.

Having reached a point where it is impossible to proceed with formal manipulations only, it is nevertheless important to recognize that for any decomposition $\mathcal{H}$, the use of the unitary operator $U_1(\tau)$ guarantees that the algorithms defined by (59)–(61b) are unconditionally stable and correct upto respectively fourth-, second-

and first order in the time step.

The Hamiltonian of a charged (spinless) non-relativistic particle in an external, static magnetic field $\mathbf{B}$ reads

$$\mathcal{H} = \frac{1}{2m^*} \left(\mathbf{p} \ - e\mathbf{A} \ \right)^2 + V \quad , \tag{62}$$

where m^* is the effective mass of the particle with charge e, $\mathbf{p} \ = -i\hbar\nabla$ is the momentum operator, $\mathbf{A}$ represents the vector potential and V denotes the potential. For many applications it is sufficient to consider the choice $\mathbf{B} \ = (0, 0, B(x, y))$ and $V = V(x, y)$. Then the problem is essentially two-dimensional and the motion of the particle may be confined to the x–y plane. For numerical work, there is no compelling reason to adopt the Coulomb gauge (div$\mathbf{A} \ = 0$). A convenient choice for the vector potential is $\mathbf{A} \ = (A_x(x, y), 0, 0)$ where

$$A_x(x, y) = -\int_0^y B(x, y)\, dy \quad . \tag{63}$$

We will solve the TDSE for the Hamiltonian (62) with the boundary condition that the wave function is zero outside the simulation box, i.e. we assume perfectly reflecting boundaries.

For computational purposes it is expedient to express all quantities in dimensionless units. Fixing the unit of length by λ, wavevectors are measured in units of $k = 2\pi/\lambda$, energies in $E = \hbar^2 k^2/2m^*$, time in $\hbar/E$ and vector potential in units of $e\lambda/\hbar$. Expressed in these dimensionless variables Hamiltonian (62) reads

$$\mathcal{H} = -\frac{1}{4\pi^2} \left\{ \left[\frac{\partial}{\partial x} - iA_x(x, y) \right]^2 + \frac{\partial^2}{\partial y^2} \right\} + V(x, y) \quad . \tag{64}$$

An essential step in the construction of a numerical algorithm is to discretize the derivatives with respect to the x and y coordinates. For our purposes, it is necessary to use a difference formula for the first and second derivatives in (64) that is accurate up to fourth order in the spatial mesh size δ. Using the standard four and five point difference formula[21] the discretized r.h.s. of (64) reads

$$\begin{aligned} H\Phi_{l,k}(t) = \frac{1}{48\pi^2\delta^2} \Big\{ & \Big[1 - i\delta\big(A_{l,k} + A_{l+2,k}\big)\Big]\Phi_{l+2,k}(t) \\ & + \Big[1 + i\delta\big(A_{l-2,k} + A_{l,k}\big)\Big]\Phi_{l-2,k}(t) \\ & - 16\Big[1 - \frac{i\delta}{2}\big(A_{l,k} + A_{l+1,k}\big)\Big]\Phi_{l+1,k}(t) \\ & - 16\Big[1 + \frac{i\delta}{2}\big(A_{l-1,k} + A_{l,k}\big)\Big]\Phi_{l-1,k}(t) \\ & + \Phi_{l,k+2} + \Phi_{l,k-2} - 16\Phi_{l,k+1} - 16\Phi_{l,k-1}(t) \end{aligned}$$

$$+\Big[60+\delta^2 A_{l,k}^2+48\pi^2\delta^2 V_{l,k}\Big]\Phi_{l,k}(t)\Big\}+\mathcal{O}(\delta^5) \quad , \qquad (65)$$

where $\Phi_{l,k}(t) = \Phi(l\delta, k\delta, t)$ and $A_{l,k} = A_x(l\delta, k\delta)$. The discretized form (65) will provide a good approximation to the continuum problem if δ is substantially smaller than the smallest physical length scale. For the case at hand there are two such scales. One is the de Broglie wavelength of the particle (which by definition is equal to λ) and the other is the (smallest) magnetic length defined by $l_B^2 = min_{(x,y)}\,|\hbar/eB(x,y)|$. From numerical calculations (not shown) it follows that $\delta = 0.1\,min(1, l_B)$ yields a good compromise between accuracy and the CPU time required to solve the TDSE.

Straightforward application of the product-formula recipe to expression (65) requires a cumbersome matrix notation. This can be avoided in the following way.[18] Defining

$$|\Phi(t)\rangle = \sum_{l=1}^{L_x}\sum_{k=1}^{L_y}\Phi_{l,k}(t)c_{l,k}^{+}|0\rangle \quad , \qquad (66)$$

where L_x and L_y are the number of grid points in the x and y direction respectively and $c_{l,k}^{+}$ creates a particle at lattice site (l,k), (66) can be written as

$$|\Phi(m\tau)\rangle = e^{-im\tau H}|\Phi(t=0)\rangle \quad , \qquad (67)$$

where

$$\begin{aligned}
H = \frac{1}{48\pi^2\delta^2}\sum_{l=1}^{L_x-2}\sum_{k=1}^{L_y}\Big\{&\Big[1-i\delta\big(A_{l,k}+A_{l+2,k}\big)\Big]c_{l,k}^{+}c_{l+2,k}\\
&+\Big[1+i\delta\big(A_{l,k}+A_{l+2,k}\big)\Big]c_{l+2,k}^{+}c_{l,k}\Big\}\\
-\frac{1}{3\pi^2\delta^2}\sum_{l=1}^{L_x-1}\sum_{k=1}^{L_y}\Big\{&\Big[1-\frac{i\delta}{2}\big(A_{l,k}+A_{l+1,k}\big)\Big]c_{l,k}^{+}c_{l+1,k}\\
&+\Big[1+\frac{i\delta}{2}\big(A_{l,k}+A_{l+1,k}\big)\Big]c_{l+1,k}^{+}c_{l,k}\Big\}\\
+\frac{1}{48\pi^2\delta^2}\sum_{l=1}^{L_x}\sum_{k=1}^{L_y-2}&\big(c_{l,k}^{+}c_{l,k+2}+c_{l,k+2}^{+}c_{l,k}\big)\\
-\frac{1}{3\pi^2\delta^2}\sum_{l=1}^{L_x}\sum_{k=1}^{L_y-1}&\big(c_{l,k}^{+}c_{l,k+1}+c_{l,k+1}^{+}c_{l,k}\big)
\end{aligned}$$

$$+\frac{1}{48\pi^2\delta^2}\sum_{l=1}^{L_x}\sum_{k=1}^{L_y}\big(60+\delta^2A_{l,k}^2+48\pi^2\delta^2V_{l,k}\big)+\mathcal{O}(\delta^5) \quad , \tag{68}$$

where $c_{l,k}$ annihilates a particle at lattice site (l,k).

Hamiltonian (68) describes a particle that moves on a two-dimensional lattice by making nearest and next-nearest neighbor jumps. This interpretation suggests that H should be written as a sum of terms that represent groups of independent jumps.[18] A convenient choice is

$$H_1=\frac{1}{48\pi^2\delta^2}\sum_{l\in X_1}\sum_{k=1}^{L_y}\Big\{\Big[1-i\delta\big(A_{l,k}+A_{l+2,k}\big)\Big]c_{l,k}^+c_{l+2,k}$$
$$+\Big[1+i\delta\big(A_{l,k}+A_{l+2,k}\big)\Big]c_{l+2,k}^+c_{l,k}\Big\} \quad ;$$
$$X_1=\{1,2,5,6,9,10,\ldots\} \quad ,$$

$$H_2=\frac{1}{48\pi^2\delta^2}\sum_{k=1}^{L_y}\sum_{l\in X_2}\Big\{\Big[1-i\delta\big(A_{l,k}+A_{l+2,k}\big)\Big]c_{l,k}^+c_{l+2,k}$$
$$+\Big[1+i\delta\big(A_{l,k}+A_{l+2,k}\big)\Big]c_{l+2,k}^+c_{l,k}\Big\} \quad ;$$
$$X_2=\{3,4,7,8,11,12,\ldots\} \quad ,$$

$$H_3=\frac{-1}{3\pi^2\delta^2}\sum_{k=1}^{L_y}\sum_{l\in X_3}\Big\{\Big[1-\frac{i\delta}{2}\big(A_{l,k}+A_{l+1,k}\big)\Big]c_{l,k}^+c_{l+1,k}$$
$$+\Big[1+\frac{i\delta}{2}\big(A_{l,k}+A_{l+1,k}\big)\Big]c_{l+1,k}^+c_{l,k}\Big\} \quad ;$$
$$X_3=\{1,3,5,7,9,11,\ldots\} \quad ,$$

$$H_4=\frac{-1}{3\pi^2\delta^2}\sum_{k=1}^{L_y}\sum_{l\in X_4}\Big\{\Big[1-\frac{i\delta}{2}\big(A_{l,k}+A_{l+1,k}\big)\Big]c_{l,k}^+c_{l+1,k}$$
$$+\Big[1+\frac{i\delta}{2}\big(A_{l,k}+A_{l+1,k}\big)\Big]c_{l+1,k}^+c_{l,k}\Big\} \quad ;$$
$$X_4=\{2,4,6,8,10,12,\ldots\} \quad ,$$

$$H_5=\frac{1}{48\pi^2\delta^2}\sum_{k\in X_5}\sum_{l=1}^{L_x}\big(c_{l,k}^+c_{l,k+2}+c_{l,k+2}^+c_{l,k}\big) \quad ; \quad X_5=\{1,2,5,6,9,10,\ldots\} \quad ,$$

$$H_6=\frac{1}{48\pi^2\delta^2}\sum_{k\in X_6}\sum_{l=1}^{L_x}\big(c_{l,k}^+c_{l,k+2}+c_{l,k+2}^+c_{l,k}\big) \quad ; \quad X_6=\{3,4,7,8,11,12,\ldots\} \quad ,$$

$$H_7 = \frac{-1}{3\pi^2\delta^2} \sum_{k\in X_7} \sum_{l=1}^{L_x} \big(c^+_{l,k}c_{l,k+1} + c^+_{l,k+1}c_{l,k}\big) \quad ; \quad X_7 = \{1,2,5,6,9,10,\ldots\} \quad ,$$

$$H_8 = \frac{-1}{3\pi^2\delta^2} \sum_{k\in X_8} \sum_{l=1}^{L_x} \big(c^+_{l,k}c_{l,k+1} + c^+_{l,k+1}c_{l,k}\big) \quad ; \quad X_8 = \{3,4,7,8,11,12,\ldots\} \quad ,$$

$$H_9 = \frac{1}{48\pi^2\delta^2} \sum_{k=1}^{L_y} \sum_{l=1}^{L_x} \big(60 + \delta^2 A^2_{l,k} + 48\pi^2\delta^2 V_{l,k}\big) \quad , \tag{69}$$

and

$$U_1(\tau) = \prod_{n=1}^{9} e^{-i\tau H_n} \quad , \tag{70}$$

is the first-order approximant from which the algorithm, correct up to fourth-order in the spatial (δ) and temporal (τ) mesh size, can be built.

Inspection of H_n for $n = 1,\ldots,9$ shows that each of the terms commutes with all the other terms in the sum over k and l. This is because each of these terms corresponds to a jump of the particle between a pair of two, isolated sites. For the purpose of implementation, this feature is of extreme importance.[18] To illustrate this point it is sufficient to consider the first of the exponents in (70) and use the fact that all terms commute to rewrite it as

$$e^{-i\tau H_1} = \prod_{k=1}^{L_y} \prod_{l\in X_1} exp\bigg(\frac{-i\tau}{48\pi^2\delta^2} \Big\{ \Big[1 - i\delta\big(A_{l,k} + A_{l+2,k}\big)\Big] c^+_{l,k}c_{l+2,k} + \Big[1 + i\delta\big(A_{l,k} + A_{l+2,k}\big)\Big] c^+_{l+2,k}c_{l,k} \Big\} \bigg) \quad . \tag{71}$$

Furthermore, each of the exponents in the product (71) describes a two-site system, and the exponent of the corresponding two-by-two matrix can be worked out analytically.[18] In general

$$\begin{aligned} exp\big(\tau\alpha c^+_{l,k}c_{l',k'} + \tau\alpha^* c^+_{l',k'}c_{l,k}\big) =& \big(c^+_{l,k}c_{l,k} + c^+_{l',k'}c_{l',k'}\big)\, cos\,\tau|\alpha| \\ & -i\big(\alpha^{*-1}c^+_{l,k}c_{l',k'} + \alpha^{-1}c^+_{l',k'}c_{l,k}\big)\, sin\,\tau|\alpha| \quad . \end{aligned} \tag{72}$$

Fortunately, the rather formal language used above easily translates into a computer program. All that (69)–(72) imply is that for each factor in product formula (70) one has to pick successive pairs of lattice points, get the values of the wave function for each pair of points and perform a plane rotation using matrices of the form

$$M = \begin{pmatrix} cos\,\tau|\alpha| & -i\alpha^{-1}\, sin\,\tau|\alpha| \\ -i\alpha^{*-1}\, sin\,\tau|\alpha| & cos\,\tau|\alpha| \end{pmatrix} \quad . \tag{73}$$

For each of the nine exponentials,[22] the order in which the pairs of points are processed is irrelevant. Therefore, the computation of each of the nine factors can be done entirely parallel, fully vectorized, or mixed parallel and vectorized depending on the computer architecture on which the code will execute. Further technical details on the implementation of this algorithm can be found elsewhere.[23]

Trotter-Suzuki based TDSE solvers have been employed to study a variety of problems including wave localization in disordered and fractals,[18,24] electron emission from nanotips,[25,26,27] Andreev reflection in mesoscopic systems,[28,29] the Aharonov-Bohm effect,[23] quantum interference of charged identical particles,[30] etc.. Appealing features of the TDSE approach are that is extremely flexible in the sense that it can handle arbitrary geometries and (vector) potentials and that its numerical stability and accuracy are such that for all practical purposes the solution is exact.

Trotter-Suzuki formala-based algorithms can and also have been used to solve the TDSE for few-body quantum systems, including a 26-site S=1/2 Heisenberg model.[31] The application of the TDSE approach is mainly limited by the storage needed for the (complex valued) wave function.

If M is so large that we cannot store the wave function other, less accurate, techniques can be used to estimate some of the dynamical properties of the model system. All these methods are based on the knowledge of certain correlation functions in the imaginary-time domain. This data is usually obtained from Quantum Monte Carlo (QMC) simulations. Straightforward extrapolation of imaginary-time data to real-time data is, from mathematical point of view, an ill-conditioned problem (i.e. numerically highly unstable) and some regularization method is required. Most successful work uses the so-called Maximum Entropy (MaxEnt) method[32] to extract spectral functions from imaginary-time QMC data. A detailed discussion of these data manipulation techniques is outside the scope of the present lecture.

6.1 Application: Quantum interference of two identical particles

Recently Silverman[33,34] proposed and analyzed a thought experiment that combines both the features of the Aharonov-Bohm (AB) and Hanbury-Brown and Twiss (HBT) experiments. The former provides information on the effect of the magnetic field on correlations of two *amplitudes*. The latter on the other hand yields direct information on the correlations of two *intensities*, i.e. of correlations of *four* amplitudes.

A schematic view of the AB-HBT apparatus is shown in Fig.1. Charged fermions or bosons leave the source S, pass through the double-slit and arrive at detectors D_1 and D_2. In order for the particle statistics to be relevant at all, it is necessary that in the detection area the wave functions of two individual particles overlap. For simplicity, it is assumed that the particles do not interact. The particle statistics

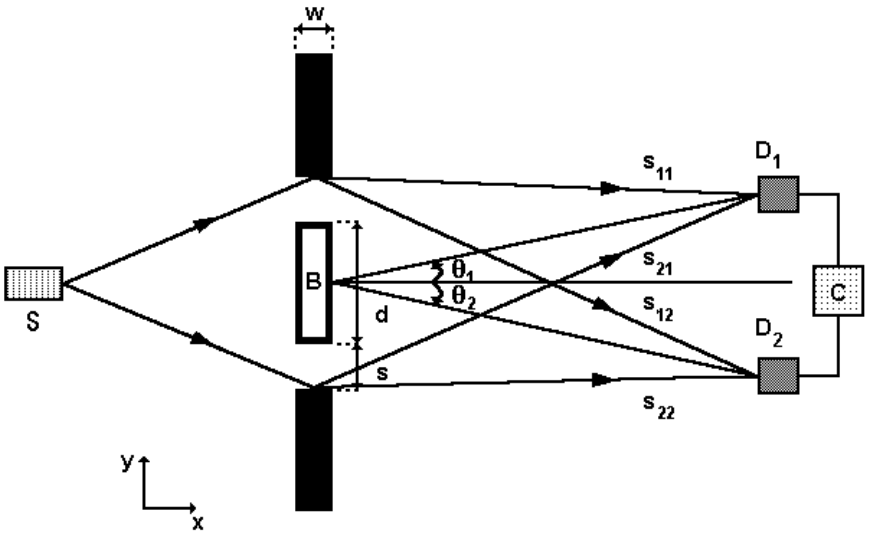

Fig.1. Schematic view of the combined Aharonov-Bohm – Hanbury-Brown Twiss apparatus. Charged fermions or bosons leave the source S, pass through the double-slit and arrive at detectors D_1 and D_2. The signals of these detectors are multiplied in correlator C. The particles do not experience the magnetic field B enclosed in the double-slit apparatus.

may affect the single-particle as well as two-particle interference. The former can be studied by considering the signal of only one of the two detectors. Information on the latter is contained in the cross-correlation of the signals of both detectors. Below we report some of our results[35] for the AB-HBT thought experiment, as obtained from the numerically exact solution of the time-dependent Schrödinger equation (TDSE) using the algorithm described above.

In practice we solve the two-particle TDSE subject to the boundary condition that the wave function is zero outside the simulation box, i.e. we assume perfectly reflecting boundaries. The algorithm that we use is accurate to fourth-order in both the spatial and temporal mesh size.[36] Additional technical details can be found elsewehere.[36] Physical properties are calculated from the two-particle amplitude $\Phi(r,r',t) = \phi_1(r,t)\phi_2(r',t) \pm \phi_2(r,t)\phi_1(r',t)$ where $\phi_1(r,t)$ and $\phi_2(r,t)$ are the single-particle amplitudes and the plus and minus sign correspond to the case of bosons and fermions respectively.

Let us first reproduce Silverman's analysis.[33,34] Assume that the double-slit apparatus can be designed such that the probability for two identical particles (fermions or bosons) to pass through the same slit can be made negligibly small. The two slits then act as the two sources in the HBT experiment with one modification: Due to the presence of the vector potential the waves can pick up an extra phase shift. According to Silverman,[33,34] it immediately follows that the signal generated by the cross-correlator will *not* show any dependence on the confined magnetic field. The AB shifts for the direct process and the one in which the identical particles

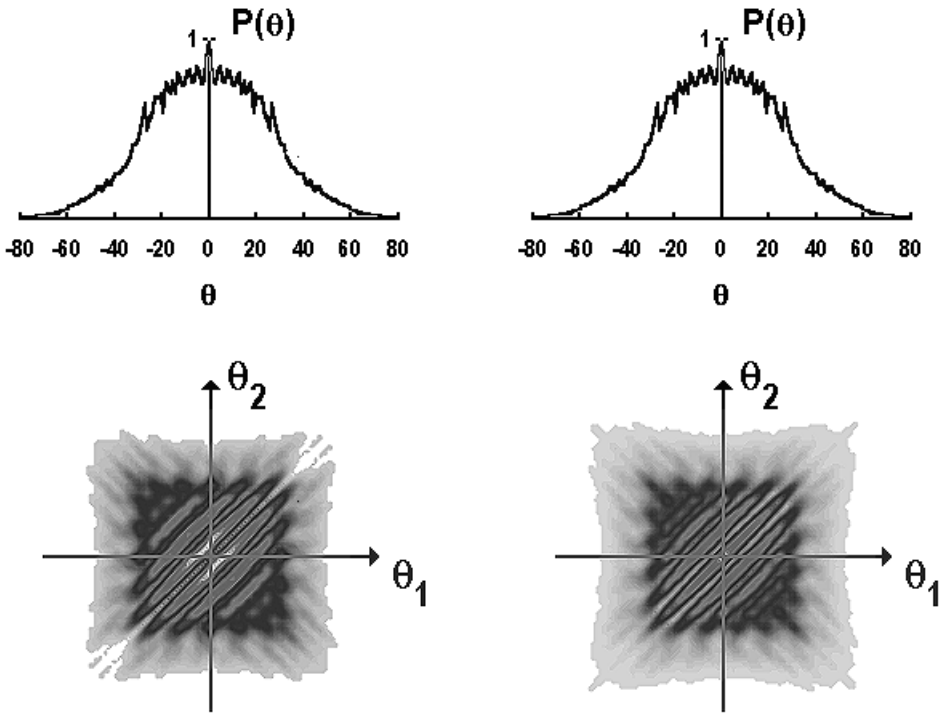

Fig.2. Simulation results for single- (top) and correlated (bottom) detector signal for $B = 0$, obtained from the solution of the TDSE for the initial state as described in the text. Left: Signals generated by fermions. Right: Signals generated by bosons. The corresponding pictures for $B = B_0$[38] are identical and not shown.

have been interchanged mutually cancel. This cancelation is independent of the fact that the particles are fermions or bosons.[37]

The basic assumption of Silverman's analysis is easily incorporated into a computer experiment. The initial two-particle wave function is a properly symmetrized product of single-particle wave functions which, for simplicity, are taken to be Gaussians. Each Gaussian is positioned such that during propagation it effectively "hits" only one slit. The single (top) and correlated (bottom) signals, received by detectors placed far to the right of the slits for $B = 0$ for fermions (l.h.s) as well as for bosons (r.h.s.) are shown in Fig.2.

For fermions the correlated signal for $\theta_1 = \theta_2$ vanishes, as required by the Pauli principle. This feature is hardly visible, due to the resolution we used to generate the pictures but it is present in the raw data. Within four digit accuracy, the corresponding data for $B = B_0$ (or, as a matter of fact, for any B) are identical to those for $B = 0$.[35] Comparison of the cross-correlated intensities (bottom part) clearly lends support to Silverman's conclusion.[33,34] However, it is also clear that the single-detector signals (upper part) do *not* exhibit the features characteristic of the AB effect. Under the conditions envisaged by Silverman, not only is there no

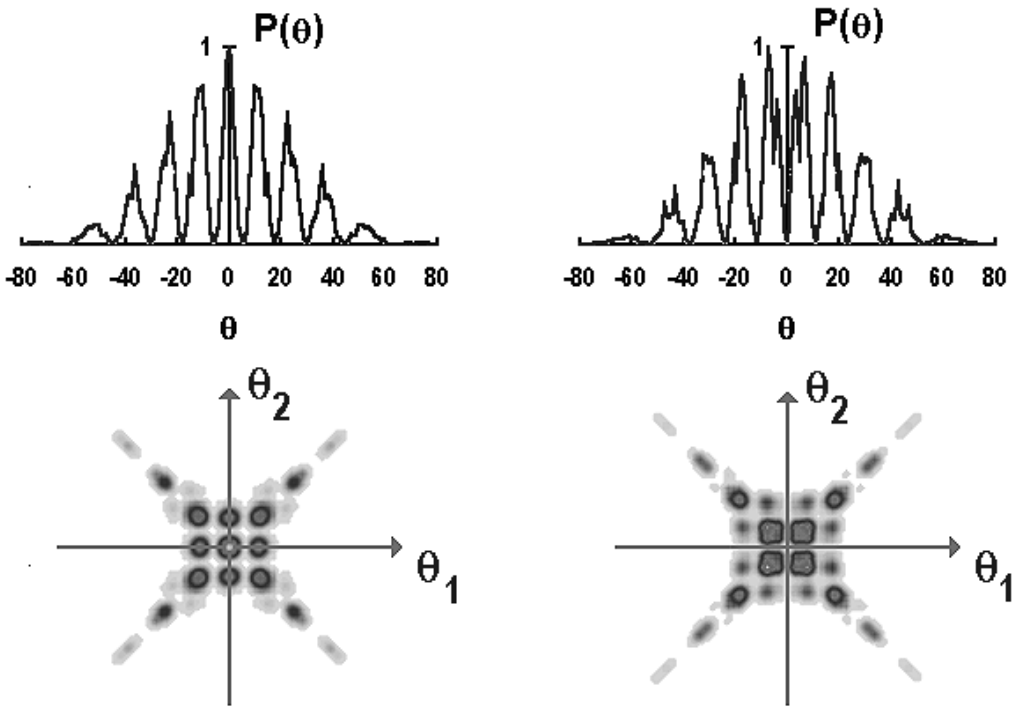

Fig.3. Simulation results for single- (top) and correlated (bottom) detector signal generated by two bosons, as obtained from the solution of the TDSE for the initial state described in the text. Left: $B = 0$. Right: $B = B_0$.

AB effect in the cross-correlated signal: There is no AB effect at all.

The absence of the AB effect can be traced back to Silvermans's assumption that the slits can be regarded as sources, thereby eliminating the second, topologically different, alternative for a particle to reach the detector. A different route to arrive at the same conclusion is to invoke gauge invariance to choose the vector potential such that the two particles would never experience a non-zero vector potential.

A full treatment of the thought experiment depicted in Fig.1 requires that *all* possibilities for *both* identical particles are included in the analysis. This is easily done in the computer experiment by changing the position and width of the Gaussians used to build the initial wave function of the fermions or bosons such that they both hit the two slits. Some of our results for the case of two bosons are shown in Fig.3. Comparison of the upper parts of Fig.3 provides direct evidence of the presence of the AB effect.

The cross-correlated boson intensities (r.h.s. of the bottom part of Fig.3) clearly exhibit an AB-like effect. The positions of the maxima and minima are interchanged if the magnetic field changes from $B = 0$ to $B = B_0$. We have verified that the shift of these positions is a periodic function of the field B. These results for the case of boson statistics cannot be explained on the basis of Silverman's theory.[33,34]

In general we find that there is only a small quantitative difference between the fermion and boson single-detector signals: The interference fringes of the fermions are less pronounced than in the case of bosons, another manifestation of the Pauli principle. The differences in the cross-correlated fermion intensities, due to B, are not as clear as in the boson case. Substracting the $B = 0$ from the $B = B_0$ signal and plotting the absolute value of this difference (not shown) clearly shows that also the cross-correlated fermion intensity exhibits features that are characteristic of the AB effect.[35] The high symmetry in all the correlated signals shown is due to our choice $B = 0, B_0$. The fact that we recover this symmetry in our simulation data provides an extra check on our method. If B is not a multiple of B_0, this high symmetry is lost but the salient features of the signals remain the same. From our numerical experiments, we conclude that in an AB-HBT experiment, an AB shift of the interference pattern will be observed in both the single and two-detector experiments. The AB effect (in both experiments) is more pronounced for bosons than for fermions.

7. Quantum Monte Carlo: Application

In this section we will discuss a particular QMC method to solve a large class of models that involve quantum particles coupled to classical degrees of freedom. Using this method one can compute the *dynamical* properties of the quantum degrees of freedom with the same accuracy as the time-independent quantities for any density of quantum particles. To illustrate the power of the method, we will present the first, numerically exact, results for the density of states and the optical conductivity of an electron-phonon model for a polymer.

From pedagogical viewpoint the method we will discuss has a number of attractive features. First of all it illustrates how QMC methods can be used to compute all physically relevant properties of a non-trivial many-body system. Secondly, the method does not suffer from the problems encountered in most QMC work: There are no minus-sign problems, time-dependent properties can be computed directly, without making use of the extrapolation techniques mentioned above, and the accuracy of the results is high. Thirdly, from methodological point of view it is complementary to the methods discussed above. Finally, it is straightforward to implement the algorithm which make it a good starting point to learn the tricks of the game.

There is a vast class of systems in all branches of many-body physics that may, as a first step, be modelled in terms of quantum mechanical degrees of freedom interacting with a set of classical variables. Models of this kind are used to describe for example, solvated electrons,[39] metallic clusters,[40] the electronic properties of polymers,[41–46] f- and d-electron systems,[47] crystallization,[48,49] etc.. Usually the classical environment itself displays complicated dynamical behavior and one often

has to resort to a Molecular Dynamics or Monte Carlo simulation to unravel its properties. Methods have been developed to incorporate the effects of the coupling of the classical variables to the quantum mechanical degrees of freedom.[39,50,51] These methods have successfully been used to compute the time-independent properties of the quantum mechanical system embedded in the classical environment.

7.1 Theory

The generic Hamiltonian of a system of fermions interacting with a set of classical degrees of freedom reads

$$H = \sum_{i,j} \sum_{s} c^{+}_{i,s} M_{i,j}(\{u_k\}) c_{j,s} + E(\{u_k\}) \quad , \tag{74}$$

where $c^{+}_{i,s}$ and $c_{i,s}$ are the creation and annihilation operators, respectively, for a fermion with spin $s =\uparrow, \downarrow$ at the generalized site (orbital) index i, u_i denotes the generalized coordinate describing the classical degrees of freedom, $M_{i,j} = M_{i,j}(\{u_k\})$ is a Hermitian matrix and $E(\{u_k\})$ represents the potential energy of the classical degrees of freedom. The grand-canonical partition function for model (74) can be written as

$$Z = Tr\ e^{-\beta(H-\mu N)} = \int_{\{u_k\}} e^{-\beta E(\{u_k\})} tr\ \ exp\left(-\beta \sum_{i,j} \sum_{s} c^{+}_{i,s} M_{i,j}\left(\{u_k\}\right) c_{j,s} \right) \quad , \tag{75}$$

where β denotes the inverse temperature and μ is the chemical potential. As already mentioned above, it is expedient to simplify (75) as much as possible by means of analytical manipulations. Since H is a quadratic form in the fermionic degrees of freedom, the trace tr over the fermions can be performed analytically as we now show. The first step is to prove the identities

$$c^{+}_{i,s}(\lambda) = e^{\lambda c^{+}\cdot M\cdot c} c^{+}_{i,s} e^{-\lambda c^{+}\cdot M\cdot c} = \sum_{j} c^{+}_{j,s} \left(e^{\lambda M}\right)_{j,i} \quad , \tag{76a}$$

$$c_{i,s}(\lambda) = e^{\lambda c^{+}\cdot M\cdot c} c_{i,s} e^{-\lambda c^{+}\cdot M\cdot c} = \sum_{j} \left(e^{-\lambda M}\right)_{i,j} c_{j,s} \quad , \tag{76b}$$

where we use the shorthand notation $c^{+}\cdot M\cdot c = \sum_{i,j}\sum_{s} c^{+}_{i,s} M_{i,j}\left(\{u_k\}\right) c_{j,s}$. To prove (76), just compute the derivative of both sides of (76a) and (76b) with respect to λ and use $c^{+}_{i,s}(\lambda = 0) = c^{+}_{i,s}$ and $c_{i,s}(\lambda = 0) = c_{i,s}$ respectively.

Next we consider a one particle state $c^{+}_{i,s}|0\rangle$ and calculate how this state changes if we operate on it with $e^{-\beta H}$. Since, by construction $c_{i,s}|0\rangle = 0$, we have

$$e^{-\beta H} c^+_{i,s}|0\rangle = e^{-\beta H} c^+_{i,s} e^{\beta H} e^{-\beta H}|0\rangle = e^{-\beta E(\{u_k\})} e^{-\beta H} c^+_{i,s} e^{\beta H}|0\rangle \quad . \tag{77}$$

We can now use (76) to obtain

$$e^{-\beta H} c^+_{i,s}|0\rangle = e^{-\beta E(\{u_k\})} \sum_j \left(e^{-\beta M}\right)_{j,i} c^+_{j,s}|0\rangle \quad . \tag{78}$$

The result (78) is readily generalized to an n-particle state, yielding

$$\begin{aligned} & e^{-\beta H} c^+_{i_1,s_1} \dots c^+_{i_n,s_n}|0\rangle \\ & \quad = e^{-\beta E(\{u_k\})} \sum_{\{j_k\}} \left(e^{-\beta M}\right)_{j_1,i_1} \dots \left(e^{-\beta M}\right)_{j_n,i_n} c^+_{j_1,s_1} \dots c^+_{j_n,s_n}|0\rangle \quad , \end{aligned} \tag{79}$$

showing the well-known fact that under the action of a Hamiltonian, quadratic in the fermionic degrees of freedom, a single Slater determinant remains a single Slater determinant. From (79) it follows that

$$\begin{aligned} & \langle 0| c_{i_1,s} \dots c_{i_n,s} e^{-\beta H} c^+_{i_1,s} \dots c^+_{i_n,s}|0\rangle = e^{-\beta E(\{u_k\})} \\ & \times \sum_{\{j_k\}} \left(e^{-\beta M}\right)_{j_1,i_1} \dots \left(e^{-\beta M}\right)_{j_n,i_n} \langle 0| c_{i_1,s} \dots c_{i_n,s} c^+_{j_1,s} \dots c^+_{j_n,s}|0\rangle \quad , \qquad (80a) \\ & = e^{-\beta E(\{u_k\})} \sum_{\{P^{(n)}\}} sign(P^{(n)}) \left(e^{-\beta M}\right)_{P^{(n)} i_1,i_1} \dots \left(e^{-\beta M}\right)_{P^{(n)} i_n,i_n} \quad , \qquad (80b) \end{aligned}$$

where $P^{(n)}$ denotes a permutation of the indices $i_1, \dots, i_n$. Including the weight $e^{-\beta\mu N}$ (i.e. working in the grand canonical ensemble) the sum over all possible numbers and arrangements of particles can be performed analytically yielding for the partition function the exact expression[15]

$$Z = \int_{\{u_i\}} \rho(\{u_i\}) = \int_{\{u_i\}} e^{-\beta E(\{u_i\})} \left[det \left(I + e^{-\beta (M(\{u_i\}) - \mu I)} \right) \right]^2 \quad , \tag{81}$$

where, as before, I denotes the unit matrix. Exact expressions for any static property of interest can be derived in a similar manner. Expectation values of static quantities are calculated as follows: For a particular configuration $\{u_i\}$ we diagonalize the $L \times L$ matrix M, compute the determinant in (81), and multiply the latter by the exponential prefactor, to obtain the weight of the configuration $\{u_i\}$. From (81) it is clear that this weight is strictly positive. Therefore it can be used in a Metropolis Monte Carlo simulation of the variables $\{u_i\}$ to calculate the averages of time-independent quantities. The algorithm is, by construction, free of minus-sign problems or numerical instabilities. This enables us to cover a much wider range of temperatures (see below) than the one which is usually accessible to other Quantum Monte Carlo methods.[52] In our implementation of the algorithm,

the computer time required to simulate the system is roughly proportional to the square of the number of lattice sites L.

We now demonstrate that for models of type (74), also the time-dependent quantities can be calculated directly, in the *real-time* domain, without invoking procedures[52] for extrapolating imaginary-time data to the real-time axis. We begin by considering the single-particle density of states

$$N(\omega) = \frac{1}{2\pi L} \sum_{l,s} \int_{-\infty}^{+\infty} d\tau e^{i\omega\tau} \langle \{c_{l,s}(\tau), c_{l,s}^{+}\} \rangle \quad , \tag{82}$$

i.e. the probability for removing or adding a single fermion from or to the system. Again using the fact that (74) is a quadratic form of the fermion operators, the time evolution of the annihilation operator in (82) can be worked out analytically (use (76) with $\lambda = i\tau$), yielding

$$\frac{1}{L} \sum_{l,s} \langle \{c_{l,s}(\tau), c_{l,s}^{+}\} \rangle = \frac{2 \int_{\{u_i\}} \rho(\{u_i\}) \, \mathbf{Sp} e^{-i\tau M(\{u_i\})}}{\int_{\{u_i\}} \rho(\{u_i\})} \quad , \tag{83}$$

where $\mathbf{Sp}X$ denotes the trace of the $L \times L$ matrix X. Since we already know the eigenvalues and eigenvectors of $M(\{u_i\})$, it is straightforward to compute the real and imaginary part of $e^{-i\tau M(\{u_i\})}$ for arbitrary τ. For each choice of τ, the calculation of $\mathbf{Sp}e^{-i\tau M(\{u_i\})}$ takes of the order of L operations (the same as for a static quantity) per configuration $\{u_i\}$, the statistical errors being comparable to those of the static quantities. In practice we choose a set of τ-values (typically 256) such that, after all samples have been taken, the integral in (82) can be computed by Fast Fourier Transformation (FFT). Thus, the total number of operations required to compute $N(\omega)$ is proportional to the number of lattice sites multiplied by the number of points in time that we use for the FFT.

The same technique can also be used to calculate other dynamical properties as well, as we now demonstrate for the case of the optical conductivity. The Kubo formula for the conductivity reads[53]

$$\sigma(\omega) = \lim_{\epsilon \to 0} \frac{i}{\omega + i\epsilon} \left\{ -\sum_{l,s} \langle [l n_{l,s}, J] \rangle + \int_0^{\infty} e^{i\omega\tau} e^{-\epsilon\tau} \langle [J, J(\tau)] \rangle d\tau \right\} \quad , \tag{84}$$

where $n_{l,s} = c_{l,s}^{+} c_{l,s}$ is the number operator for site l and spin s, and the current operator is given by $J = i \sum_{l,s} [H, l n_{l,s}]$. It is straightforward to work out analytically, the time-evolution of $J(\tau)$ and the commutator appearing in (84). The resulting expression for the integrand is used to sample the current-current correlation function for a set of τ-values (typically 512). After collecting all data, application of the FFT yields the frequency-dependent conductivity. Unlike for the density of states,

the computation time per τ-value is not a linear function of L but increases with the third power of L, effectively limiting the system size that we can study to $L \leq 256$. The statistical noise on the conductivity is of the same order of magnitude as for the density of states and the static quantities. Disregarding the statistical errors (which are too small to be visible on the figures presented below) the results for the static and dynamic properties are, for all practical purposes, numerically exact.

7.2 Hubbard-Stratonovitch Transformation

Can we compute the properties of more complicated fermion systems in the same way ? The answer is no and the reason is the following. In our derivations we heavily relied on the fact that generic model (74) is a quadratic form of the fermion operators. If we add to (74) a term that accounts for a direct interaction between the fermions then things become much more complicated.

As an example let us consider adding to (74) a "Hubbard" interaction

$$H_{Hub} = U \sum_i n_{i,\uparrow} n_{i,\downarrow} \quad . \tag{85}$$

where U is the so-called on-site Coulomb interaction strength. If we replace H by $H + H_{Hub}$ then (78) – (81) no longer hold because the new H now contains quartic terms. We can get around this problem by invoking the Trotter-Suzuki formula

$$e^{-\tau(H+H_{Hub})} \approx e^{-\tau H} e^{-\tau H_{Hub}} \quad , \tag{86}$$

where we have assume that $\tau = \beta/m > 0$ is sufficiently small, and the identities

$$e^{-\tau H_{Hub}} = \prod_i e^{-\tau U n_{i,\uparrow} n_{i,\downarrow}} = \prod_i e^{\tau U (n_{i,\uparrow} - n_{i,\downarrow})^2/2} e^{-\tau U (n_{i,\uparrow} + n_{i,\downarrow})/2} \quad , \tag{87a}$$

$$= \prod_i \sqrt{2\tau\pi U} \int_{-\infty}^{+\infty} dx_i \; e^{-x_i^2/2\tau U - x_i (n_{i,\uparrow} - n_{i,\downarrow}) - \tau U (n_{i,\uparrow} + n_{i,\downarrow})/2} \quad , \tag{87b}$$

$$= \prod_i \frac{1}{2} \sum_{\sigma_i = \pm 1} e^{\tau^* \sigma_i (n_{i,\uparrow} - n_{i,\downarrow})} e^{-\tau U (n_{i,\uparrow} + n_{i,\downarrow})/2} \quad , \tag{87c}$$

where $cosh\, \tau^* = e^{\tau U/2}$ and $U > 0$. Representation (87b) is obtained by using (5.4). The trick of expressing the exponential of an two-particle interaction as an integral over auxilary variables ($\{x_i\}$ in our case) is usually called the Hubbard-Stratonovitch transformation. The discrete form (87c) is due to Hirsch.[54] Expressions for $U < 0$ can be derived in the same manner.

From (87b) or (87c) it is clear that we have now written $e^{-\tau H_{Hub}}$ as a sum of exponentials of *quadratic* forms of the fermion operators. Now we are in the position to use (79) and obtain

$$\left(e^{-\beta H/m}e^{-\beta H_{Hub}/m}\right)^m c^+_{i_1,s}\dots c^+_{i_n,s}|0\rangle$$
$$=e^{-\beta E(\{u_k\})}\sum_{\{j_k\}} A^{(s)}_{j_1,i_1}\dots A^{(s)}_{j_n,i_n} c^+_{j_1,s}\dots c^+_{j_n,s}|0\rangle \quad , (88a)$$

where

$$A^{(s)} =2^{-mL}e^{-\tau M}e^{sD(\{\sigma_{i,1}\})}\dots e^{-\tau M}e^{sD(\{\sigma_{i,m}\})} \quad , \qquad (88b)$$

and

$$D(\{\sigma_{i,k}\})_{l,l'} =\tau^*\sigma_{l,k}\delta_{l,l'} \quad , \qquad (88c)$$

where for concreteness we have used the discrete representation (87c) . The result (88) can now be used derive the expression of the partition function in the grand canonical ensemble. The exact expression reads

$$Z=\int_{\{u_i\}} e^{-\beta E(\{u_i\})}\sum_{\{\sigma_{i,j}=\pm 1\}} det\left(I+A^{(1)}\right) det\left(I+A^{(-1)}\right) \quad . \qquad (89)$$

At first sight, (89) looks very similar to (81) but this is only due to our use of a compact notation. The matrices $A(s)$, as defined in (88b) are complicated objects. Although still real, they are no longer symmetric and hence there is no guarantuee that for a given realization of the $\{\sigma_{i,j}\}$, the product of the determinants is positive. This is nothing but another manifestation the minus-sign problem. This example shows that even if we do our best to perform the sum over all fermionic degrees of freedom, the fact that we had to make use of a product formula at some stage of the calculation results in minus-sign problems. More details on how one can proceed anyway can be found elsewhere.[13,15,52]

7.3 Application

We now return to the more simple case of the generic model (74) and as an illustration we will apply the method described above to the Su, Schrieffer, and Heeger (SSH) model for trans-polyacetylene.[41–46] Application to models for correlated electrons can be found elsewhere.[55–61] The SSH Hamiltonian reads

$$H=-\sum_i\sum_s \left(t-\alpha\left(u_{i+1}-u_i\right)\right)\left(c^+_{i,s}c_{i+1,s}+c^+_{i+1,s}c_{i,s}\right)$$
$$+\frac{K}{2}\sum_i\left(u_{i+1}-u_i\right)^2 \quad , \qquad (90)$$

where $c^+_{i,s}$ and $c_{i,s}$ are the creation and annihilation operators, respectively, for a π-electron with spin $s =\uparrow,\downarrow$ at the i-th CH group, $n_{i,s}$ denotes the number operator at group i, μ is the chemical potential which fixes the number of π-electrons, u_i is the coordinate describing the displacement of the i-th CH group along the molecular symmetry axis, t is the hopping integral for the undimerized chain, α is the electron-phonon coupling constant and K is the effective σ-spring constant.[41−46] The absence, in (90), of the lattice kinetic energy implies that the displacements may be regarded as classical degrees of freedom, a good starting point for the description of the electronic properties of polyacetylene.[41−46]

Model Hamiltonian (90) clearly falls into the class of models described by the generic Hamiltonian (79). For the SSH model, $E(\{u_k\}) = (K/2)\sum_i (u_{i+1} - u_i)^2$, $M_{i,j}(\{u_k\}) = -t + \alpha(u_j - u_i)$ for i, j nearest neighbors, and $M_{i,j}(\{u_k\}) = 0$ otherwise. The current operator of the SSH model is given by

$$J = i\sum_{i,s} \left(-t + \alpha(u_{i+1} - u_i)\right)\left(c^+_{i,s}c_{i+1,s} - c^+_{i+1,s}c_{i,s}\right) \quad . \tag{91}$$

Our approach differs from others[41−46] in that it allows a *first-principle* calculation of the static and dynamic properties of (91). It does not depend on a particular variational ansatz for the u_i configuration nor is there the risk of ending up in a local instead of global minimum of the (free) energy. Furthermore, to the best of our knowledge, it yields the first *first-principle* calculation of the optical conductivity of model (91).

The results reported below have been obtained from simulations of rings containing up to 256 sites (CH groups) and 256 electrons, exceeding the length of most chains in actual materials,[62−64] for a set of model parameters appropriate for polyacetylene[42−46] : $t = 2.5eV$, $\alpha = 4.1eV/Å$ and $K = 21eV/Å^2$. Energies will be measured in units of $t = 2.5eV$. We show results for even-site chains only and we confine ourselves to a discussion of low-temperature results (in practice we set $T = 2.9K$, corresponding to $\beta t = 10000$).[65]

First we demonstrate that our method reproduces the known features of the model.[41−46] At half-filling the Peierls instability[66] leads to a dimerization, adjacent CH groups forming alternately short and long bonds. Our numerical results for a half-filled CH chain show that the distortion parameter $u_0 \equiv |\sum_i (-1)^i \langle u_i\rangle|/2L = 0.0396Å$. In Fig.4 we show the pattern of the lattice displacement for a dopant concentration $y \equiv 1 - n = 0.016$, where n is the density of electrons in the chain. The small oscillations on top of a superstructure can easily be removed by standard filtering procedures. The result is depicted in Fig.5.

The solid curve in Fig.4 is given by $u_i = u_0\, tanh[(i - i_0)/l]$ where i_0 is a fitting parameter, $l = 8$ determines the extent of the defect and $u_0 = 0.0396Å$. The hyperbolic tangent is characteristic of the bond-length alternation associated with the geometric distortion due to a soliton on an infinite chain.[41−46] Variational

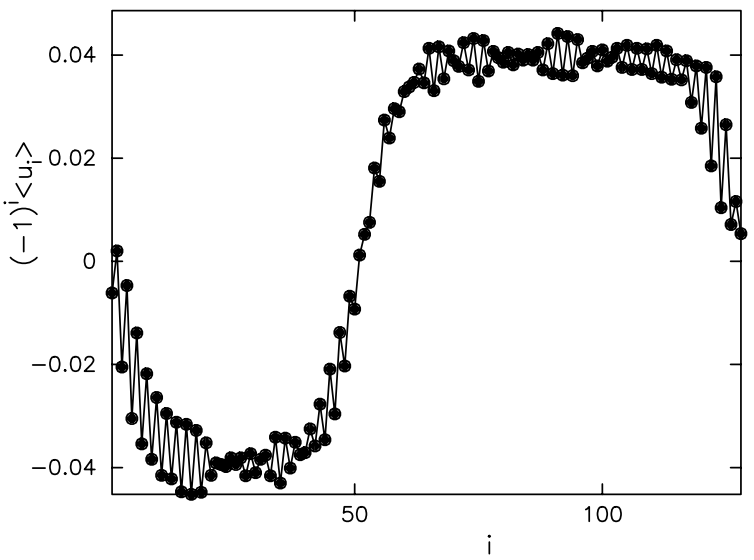

Fig.4. Lattice distortions for a ring of 128 sites for $y = 0.016$. The line is a guide to the eye.

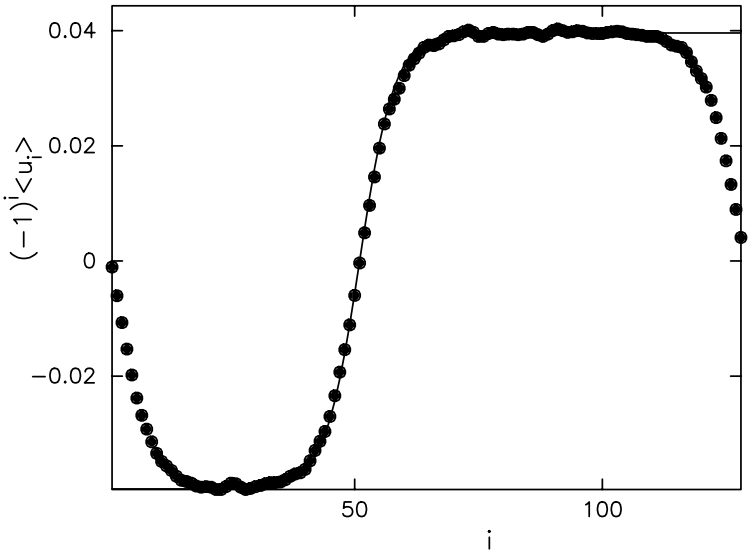

Fig.5. Same as Fig.4, but the smallest wave numbers are filtered out. Bullets: Simulation results; solid line: $u_0\, tanh\,[(i - i_0)/l]$.

calculations suggest a value of $l \approx 7$.[42–46] As expected, Figs.4,5 shows that for the case in which two electrons are taken away from a half-filled 128-site ring, two solitons are being created.

Upon doping the system further the soliton lattice evolves toward a sinusoidal modulation as shown in Figs.6,7 for $y = 0.078$. The solid curve in Fig.7 is given by $u_i = u_0\, sin[2\pi m(i - i_0)/L]$, where i_0 and m are fitting parameters. Additional

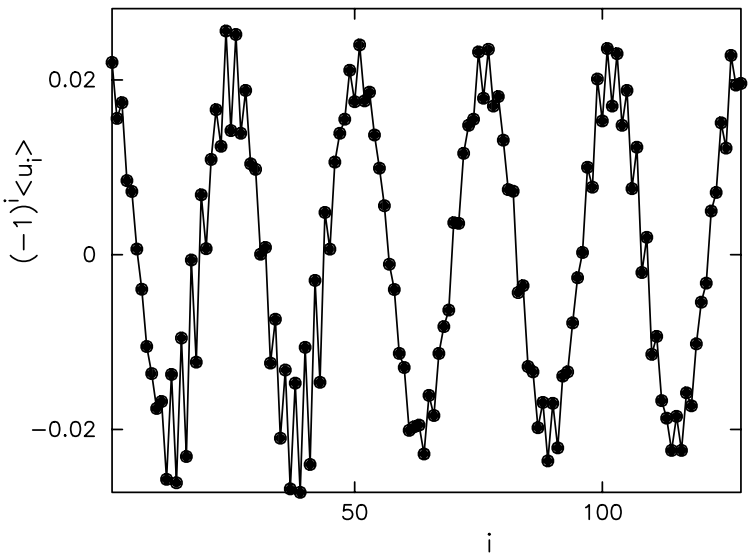

Fig.6. Lattice distortions for a ring of 128 sites for $y = 0.078$. The line is a guide to the eye.

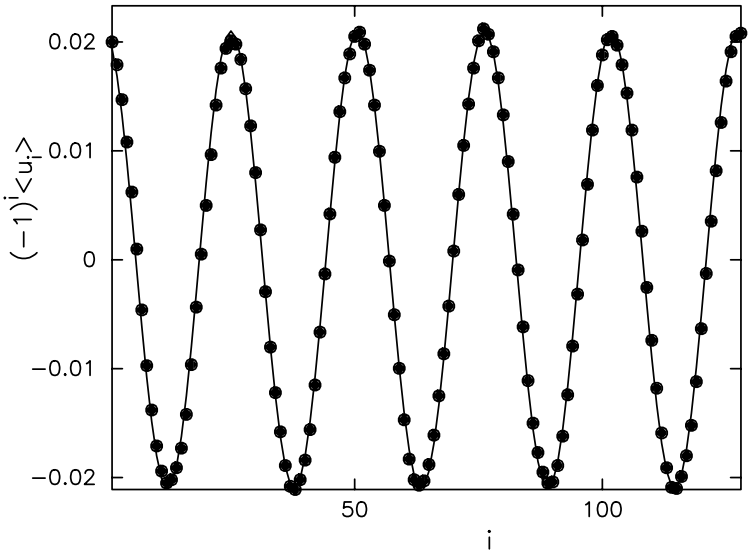

Fig.7. Same as Fig.6, but the smallest wave numbers are filtered out. Bullets: Simulation results; solid line: $u_0\, sin\,[2\pi m(i - i_0)/L]$.

simulations for 256-site rings (results not shown) strongly suggest that solitons (soliton-antisoliton pairs) are only present for dopant concentrations $y < 0.031$ and that the transition from the soliton lattice to the sinusoidal modulation is continuous.

There is strong experimental evidence that upon doping trans-polyacetylene a first-order phase transition occurs at a dopant concentration of approximately

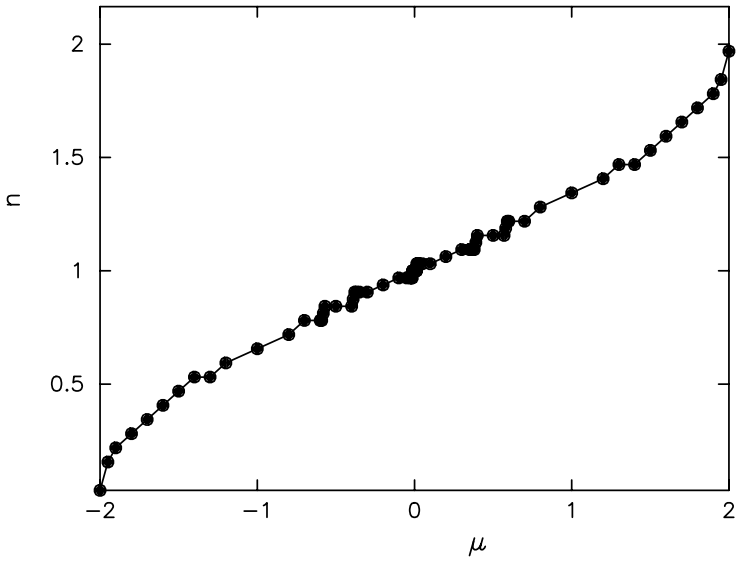

Fig.8. Electron density n as a function of the chemical potential μ for a ring of 256 sites. The line is a guide to the eye.

6%.[67−64] A first-order phase transition is characterized by plateau's and steps in n versus μ.[69] Since we perform our calculations in the grand-canonical ensemble we only have to compute the density n for many values of the chemical potential μ. Our numerical results, depicted in Fig.8, show that n varies smoothly as a function of μ, strongly suggesting that the SSH model does not exhibit a first-order transition as a function of doping. The small steps in n versus μ indicate that only states with an even number of electrons are thermodynamically stable and that the formation of polarons is unlikely. This also implies (and is corroborated by our simulation data (not shown)) that systems of 64 sites or less cannot support soliton–antisoliton pairs because the removal of two electrons from the half-filled system corresponds to a dopant concentration that exceeds the critical value of 3.1%.

In Fig.9 we show $N(\omega)$ for a ring of 256 sites for various dopant concentrations. The position of the chemical potential is indicated by the dashed line. For half filling ($y = 0$), $N(\omega)$ consists of two bands separated by a gap $\Delta = 1eV \pm 0.3eV$. The chemical potential is located in the middle of the gap and the system acts as a dimerized semiconductor. At low dopant concentration ($y < 0.06$) there is a narrow, mid-gap band in the density of states. For $y \leq 0.031$ this band is due to the presence of solitons whereas for $0.031 < y \leq 0.06$ it results from the sinusoidal modulation. At high dopant concentration ($y > 0.06$) the midgap-band broadens. In the doped system the chemical potential always falls in a gap. There is excellent qualitative agreement between the results for the density of states obtained by a combination of geometry optimization and the continued fraction technique[70,71] and our numerically exact results.

Fig.10 shows a series of calculated absorption spectra for various dopant con-

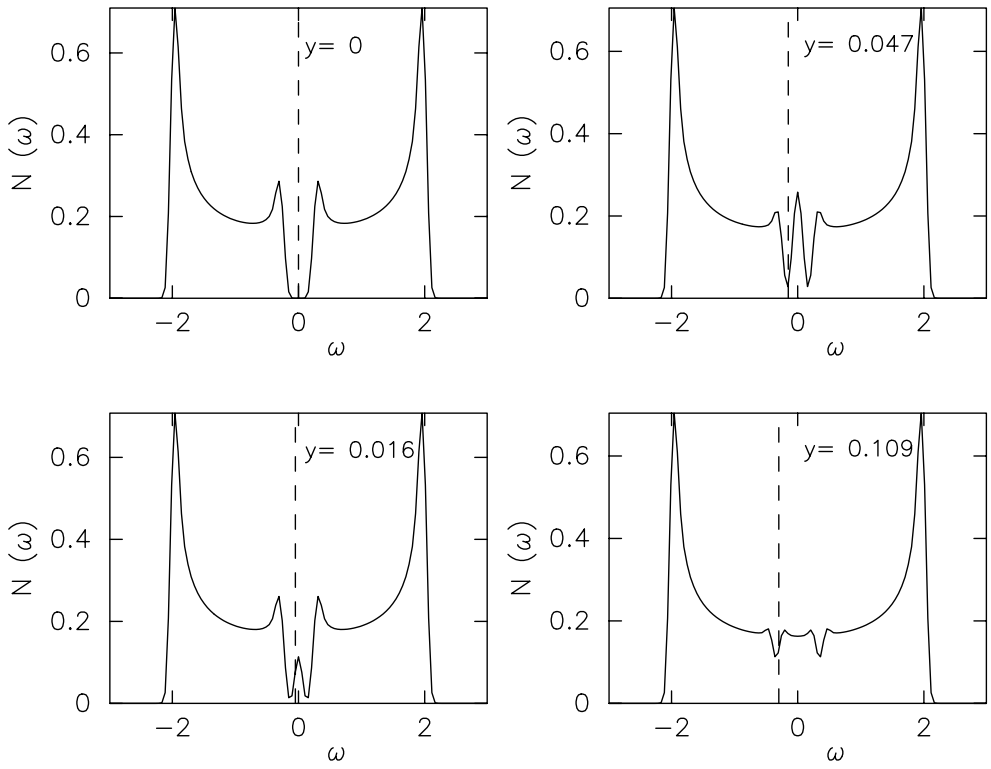

Fig.9. Density of states $N(\omega)$ for a ring of 256 sites for various dopant concentrations y. The dashed line denotes the position of the chemical potential.

centrations. The optical absorption for the undoped case (thick solid line) has a gap which is as broad as the gap in the density of states. For dopant concentrations below 6%, a midgap absorption peak appears. The intensity of the midgap absorption peak comes from the interband transitions over the whole spectral range. For $y < 0.031$, i.e. the range of dopant concentrations for which the system supports solitons, the intensity of the midgap absorption is proportional to the dopant concentration. In the intermediate doping regime $0.031 < y < 0.06$, the doping dependence of the intensity of the midgap absorption changes. In the heavily doped regime ($y > 0.06$) the interband transition has completely disappeared. Our calculations of the optical absorption reproduce all salient features observed experimentally.[72−74]

8. Acknowledgements

I would like to thank K. Michielsen for a critical reading of the manuscript. Financial support by the "Stichting voor Fundamenteel Onderzoek der Materie (FOM)", which is financially supported by the "Nederlandse Organisatie voor Wetenschappelijk Onderzoek (NWO)", the "Stichting Nationale Computer Faciliteiten

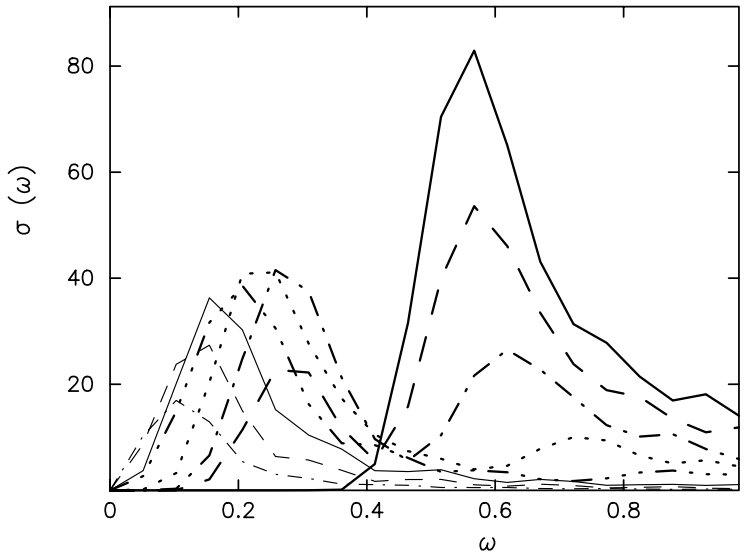

Fig.10. Optical absorption $\sigma(\omega)$ for a ring of 128 sites for various dopant concentrations. Thick solid line: $y = 0$, thick dashed line: $y = 0.016$, thick dash-dotted line: $y = 0.031$, thick dotted line: $y = 0.047$, thick dash-triple dotted line: $y = 0.063$, thin solid line: $y = 0.078$, thin dashed line: $y = 0.109$, thin dash-dotted line: $y = 0.328$.

(NCF)", and the EEC is gratefully acknowledged.

9. References

1. J.H. Wilkinson, *The Algebraic Eigenvalue Problem*, (Clarendon Press, Oxford 1965).
2. B.N. Parlett, *The Symmetric Eigenvalue Problem*, (Prentice-Hall,New Jersey 1981).
3. K.E. Schmidt and M.H. Kalos, *Applications of the Monte Carlo Methods in Statistical Physics*, edited by K. Binder, (Topics in Current Physics 36, Springer, Berlin, 1984).
4. E.R. Davidson, *J. Comp. Phys.* **17** (1975) 87.
5. J. Olsen, P. Jørgensen, and J. Simons, *Chem. Phys. Lett.* **169** (1990) 463.
6. G.H. Golub, and C.F. Van Loan, *Matrix Computations*, (John Hopkins University Press, Baltimore 1983).
7. E.R. Gagliano, E. Dagotto, A. Moreo, and F.C. Alcaraz, *Phys. Rev.* **B34** (1986) 1677.
8. M.P. Nightingale, V.S. Viswanath, and G. Müller, *Phys. Rev.* **B48** (1993) 7696.
9. H. De Raedt, and W. von der Linden, *Phys. Rev.* **B45** (1992) 8787.
10. H. De Raedt, and M. Frick, *Phys. Rep.* **231** (1993) 107.

11. L. Visscher, H. De Raedt, and W.C. Nieuwpoort, *Chem. Phys. Lett.* **227** (1994) 327.
12. S. Lie and F. Engel, *Theorie der Transformationgruppen*, (Teubner, Leipzig 1888).
13. H. De Raedt, and A. Lagendijk, *Phys. Rep.* **127** (1985) 233.
14. M. Suzuki, *Quantum Monte Carlo Methods*, edited by M. Suzuki, (Solid State Sciences 74, Springer, Berlin, 1986).
15. H. De Raedt and W. von der Linden, *Monte Carlo Methods in Condensed Matter Physics*, edited by K. Binder, (Springer, Berlin, 1992).
16. M. Suzuki, *J. Math. Phys.* **601** (1985) 26.
17. R.P. Feynman, and A.R. Hibbs, *Quantum Mechanics and Path Integrals*, (McGraw-Hill, New York 1965).
18. H. De Raedt, *Comp. Phys. Rep.* **7** (1987) 1.
19. M. Suzuki, *J. Math. Phys.* **32** (1991) 400.
20. H. De Raedt, and B. De Raedt, *Phys. Rev.* **A28** (1983) 3575.
21. M. Abramowitz and I. Stegun, *Handbook of Mathematical Functions*, (Dover, New York 1964).
22. The case $n = 9$ is even simpler than the other eight cases but for the sake of brevity, a discussion of this detail is omitted.
23. H. De Raedt, and K. Michielsen , *Computers in Physics* **8** (1994) 600.
24. P. de Vries, H. De Raedt, and A. Lagendijk, *Comp. Phys. Commun.* **75** (1993) 298.
25. N. García, J.J. Sáenz, and H. De Raedt, *J. Phys.: Condens. Matter* **1** (1989) 9931.
26. H. De Raedt, and K. Michielsen, *Nanoscources and Manipulation of Atoms Under High Fields and Temperatures: Applications*, edited by Vu Thien Binh, N. García and K. Dransfeld, (NATO-ASI Series, Kluwer, 1993).
27. K. Michielsen and H. De Raedt, "Electron Focussing", MultiMedia Presentation.
28. H. De Raedt, K. Michielsen, and T.M. Klapwijk, *Phys. Rev.* **B50** (1994) 631.
29. H. De Raedt and K. Michielsen, "Andreev Reflection", MultiMedia Presentation.
30. H. De Raedt, and K. Michielsen, Annalen der Physik (in press).
31. P. de Vries, and H. De Raedt, *Phys. Rev.* **B47** (1993) 7929.
32. B. Buck, and V.A. Macauly, *Maximum Entropy in Action*, (Clarendon, Oxford 1991).
33. M.P. Silverman, *Am. J. Phys.* **61** (1993) 514.
34. M.P. Silverman, *And Yet It Moves: Strange Systems and Subtle Questions in Physics* , (Cambridge, New York 1993).
35. H. De Raedt, and K. Michielsen, *Annalen der Physik* (in press).

36. H. De Raedt, and K. Michielsen, *Computers in Physics* **8** (1994) 600.
37. M.P. Silverman, private communication.
38. B_0 is the magnetic field for which the Aharonov-Bohm shift of the interference pattern is equal to π.
39. A. Alavi, and D. Frenkel, *J. Chem. Phys.* **97** (1992) 9249.
40. A. Yoshida, T. Døssing, and M. Manninen, *J. Chem. Phys.* **101** (1994) 3041.
41. M.J. Rice, *Phys. Lett.* **71A** (1979) 152.
42. W.P. Su, J.R. Schrieffer, and A.J. Heeger, *Phys. Rev. Lett.* **42** (1979) 1698.
43. W.P. Su, J.R. Schrieffer, and A.J. Heeger, *Phys. Rev.* **B22** (1980) 2209.
44. W.P. Su, J.R. Schrieffer, and A.J. Heeger, *Phys. Rev.* **B28** (1983) 1138.
45. A.J. Heeger, S. Kivelson, J.R. Schrieffer, and W.-P. Su, *Rev. Mod. Phys.* **60** (1988) 781.
46. Yu Lu, *Solitons & Polarons in Conducting Polymers*, (World Scientific, Singapore 1988).
47. L.M. Falicov, and J.C. Kimball, *Phys. Rev. Lett.* **22** (1969) 997.
48. T. Kennedy, and E.H. Lieb, *Physica* **A138** (1986) 320.
49. J. Jedrzejewski, J. Lach, and R. Lyzwa, *Physica* **A154** (1989) 529.
50. R. Car, and M. Parinello, *Phys. Rev. Lett.* **55** (1985) 2471.
51. A. Alavi, J. Kohanoff, M. Parinello, and D. Frenkel, *Phys. Rev. Lett.* **73** (1994) 2599.
52. W. von der Linden, *Phys. Rep.* **220** (1992) 53.
53. R. Kubo, *J. Phys. Soc. Jpn.* **12** (1957) 570.
54. J.E. Hirsch, *Phys. Rev.* **B31** (1985) 4403.
55. K. Michielsen, H. De Raedt, and T. Schneider, *Phys. Rev. Lett.* **68** (1992) 1410.
56. K. Michielsen, *Int. J. Mod. Phys.* **B7** (1993) 2571.
57. P. de Vries, K. Michielsen, and H. De Raedt, *Phys. Rev. Lett.* **70** (1993) 2463.
58. P. De Vries, K. Michielsen, and H. De Raedt, *Z. Phys.* **B92** (1993) 353.
59. K. Michielsen, H. De Raedt, T. Schneider, and P. de Vries, *Europhys. Lett.* **25** (1994) 599.
60. P. de Vries, K. Michielsen and H. De Raedt, *Z. Phys.* **B95** (1994) 475.
61. K. Michielsen, and H. De Raedt, *Phys. Rev.* **E50** (1994) 4371.
62. J.E.Hirsch, and M. Grabowski, *Phys. Rev. Lett.* **52** (1984) 1713.
63. H. Thomann, L.R. Dalton, Y. Tomkiewicz, N.S. Shiren and T.C. Clarke, *Phys. Rev. Lett.* **50** (1983) 533.
64. M. Winokur, Y.B. Moon, A.J. Heeger, J. Barker, D.C. Bott, and H. Shirakawa, *Phys. Rev. Lett.* **58** (1987) 2329.
65. Data for odd-site chains and room temperature will be published elsewhere.
66. R.E. Peierls, *Quantum Theory of Solids*, (Clarendon Press, Oxford 1955).
67. J. Chen, T.-C. Chung, F. Moraes, and A.J. Heeger, *Sol. Stat. Comm.* **53**

(1985) 757.
68. F. Moraes, J. Chen, T.-C. Chung, and A.J. Heeger, *Synth. Met.* **11** (1985) 271.
69. L.E. Reichl, *A Modern Course in Statistical Physics*, (Edward Arnold, London 1980).
70. E.J. Mele, and M.J. Rice, *Phys. Rev.* **B23** (1981) 5397.
71. M.J. Rice, and E.J. Mele, *Chem. Scr.* **17** (1981) 121.
72. H. Suzuki, M. Ozaki, S. Etemad, A.J. Heeger, and A.G. Mac-Diarmid, *Phys. Rev. Lett.* **45** (1980) 1209.
73. A. Feldblum, J.H. Kaufman, S. Etemad, and A.J. Heeger, *Phys. Rev.* **B26** (1982) 815.
74. T.-C. Chung, F. Moreas, J.D. Flood, and A.J. Heeger, *Phys. Rev.* **B29** (1984) 2341.

Contents:

1. Introduction 1
2. Exact Diagonalization 3
   - 2.1 Methods to compute the full spectrum 3
   - 2.2 Methods to compute the part of spectrum 4
   - 2.2 Projector methods 4
   - 2.2 Subspace iteration 6
3. Variational Methods 8
   - 3.1 Fundamental Theorems 8
   - 3.2 Trial State Approach 9
   - 3.3 Recursive Variational Techniques 9
   - 3.4 Stochastic Diagonalization 11
   - 3.5 Computation of physical properties 12
4. Trotter-Suzuki Formulae 12
5. Path Integrals 17
6. Quantum Dynamics 20
   - 6.1 Application: Quantum interference of two identical particles . 26
7. Quantum Monte Carlo: Application 30
   - 7.1 Theory 31
   - 7.2 Hubbard-Stratonovitch Transformation 34
   - 7.3 Application 35
8. Acknowledgements 40
9. References 40